Journal of Nanobiotechnology

RESEARCH

Open Access

Radiotherapy-derived engineered stem cell exosomes improve anti-glioma immunotherapy by promoting the formation of tertiary lymphoid structure and improve the release of type I interferon

Man Li[1,2†], Lisen Lu[3†], Qiuhong Bao[4†], Minghui Zhou[1], Bin Nie[2], Yanchao Liu[1], Kai Shu[1], Ting Lei[1] and Mingxin Zhu[1*]

Abstract

The absence of signaling pathways related to intrinsic immune activation in tumor cells and the immunosuppressive microenvironment limit lymphocyte infiltration, constitutes an "immune-desert" tumor displaying insensitivity to various immunotherapies. This study investigates strategies to activate intrinsic immune pathways in glioma cells, reverse immunosuppression, and induce tertiary lymphoid structures (TLS) within the glioma microenvironment (GME) to enhance natural and adaptive immune responses. We successfully induced antigen-presenting cell activation, macrophage/microglia polarization, and TLS formation in GME by intracranial delivery of BafA1@Rexo-SC, which comprises exosomes from irradiated bone marrow-derived stem cells overexpressing CD47 nanobodies and STING, loaded with the autophagy inhibitor BafA1. These exosomes efficiently activated the cGAS-STING pathway, leading to the formation of "lymphoid tissue organizer cells (Lto)" cells, VEGFA release for high endothelial microvessel formation, and chemokine release for T and B cell recruitment. BafA1@Rexo-SC also promoted macrophage phagocytosis of tumor cells and enhanced effector T cell function by blocking CD47, while releasing type I interferon. Our findings suggest novel therapeutic approaches for glioma treatment.

Keywords Tertiary lymphoid structures, cGAS-STING, Exosomes, Stem cells, Glioma, Tumor microenvironment

†Man Li, Lisen Lu and Qiuhong Bao contributed equally to this work.

*Correspondence:
Mingxin Zhu
mxzhu@tjh.tjmu.edu.cn
Full list of author information is available at the end of the article

Graphical abstract

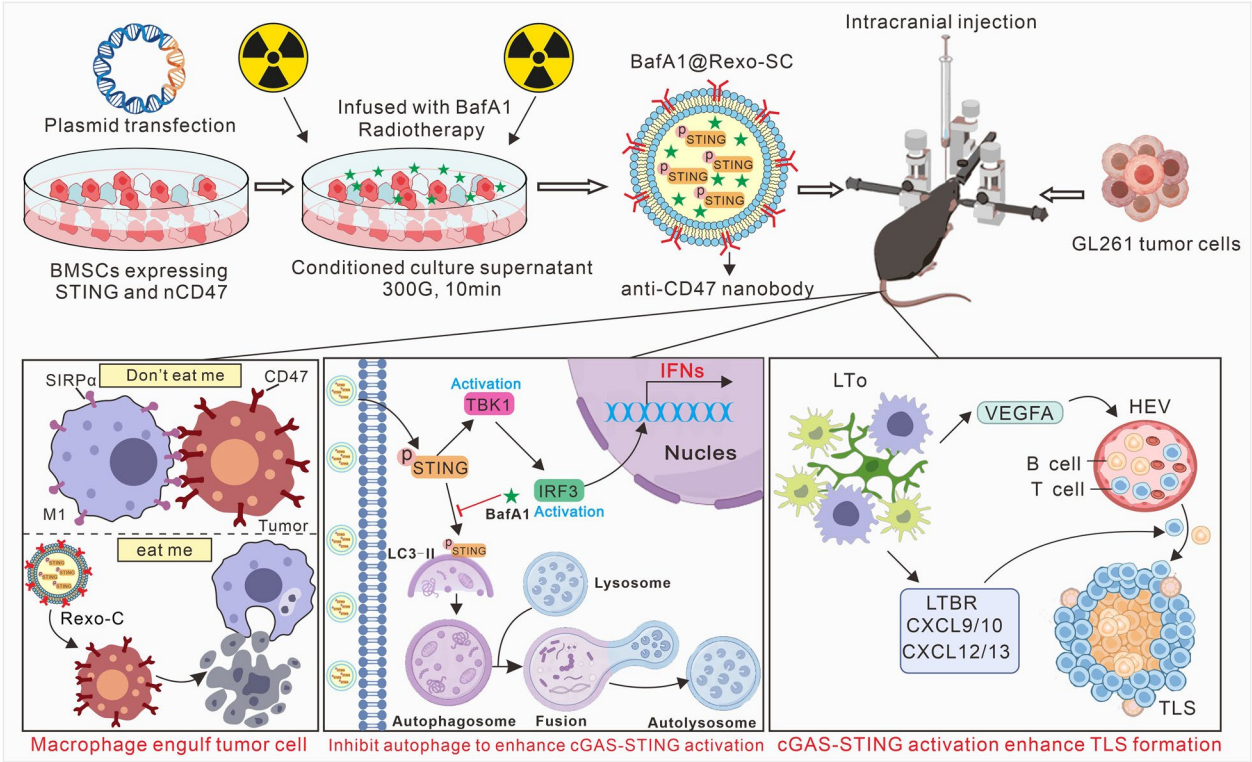

Introduction

Immunotherapy has brought a turning point in the treatment of numerous human solid tumors and has also kindled hope for the immunotherapy of glioma [1]. A series of studies on immunotherapy for glioblastoma multiforme (GBM) have been initiated [2]. However, less than 20% of glioma patients derive lasting clinical benefits from these immunotherapies [3]. Among various immunotherapies, tumor-infiltrating lymphocytes (TILs) also struggle to infiltrate the glioma microenvironment (GME) [4]. Therefore, novel immunotherapies that promote TIL infiltration into GME, thereby shifting GME from a state of immune resistance to activation, may yield significant outcomes.

In the anti-tumor immune cycle, the initiation and activation of lymphocytes are crucial for the formation of anti-tumor immunity, a process that typically occurs in secondary lymphoid organs (SLOs) such as lymph nodes [5]. Recent studies have indicated that this step can also be accomplished in tertiary lymphoid structures (TLS) [6]. Structurally, TLS are similar to SLOs, comprising T cell zones and follicular B cell areas. Mature TLS even contain germinal centers (GCs), which can serve as surrogates for SLOs and promote the occurrence of adaptive immune responses in the disease microenvironment [7]. To date, the induced formation of TLS has been observed in various tumor microenvironments (TMEs), and their distribution density correlates with T lymphocyte infiltration in TMEs, improvement in prognosis, and enhancement of clinical outcomes following other immunotherapies [8]. The generation of tertiary lymphoid structures in glioma also significantly extends the survival rate of orthotopic glioma model mice. However, current methods to promote the formation of TLS mainly involve direct injection of TLR agonists or AAV infection in the brain, which cannot avoid nonspecific activation of the normal central nervous system [9, 10]. Moreover, the epigenetic and metabolic plasticity of glioma cells, which mediate low immunogenicity, can resist the immune system activation mediated by TLS [11, 12]. Thus, strategies that can simultaneously regulate the formation of TLS in the tumor microenvironment and the immunogenicity of tumor cells themselves, without damaging the central nervous system, may become the main direction for the clinical treatment of glioma patients in the future.

The cGAS-STING signaling pathway plays a crucial role in antiviral and antitumor immunity, particularly in the activation of innate immune cells such as dendritic cells and macrophages. It functions by secreting type I interferons and other pro-inflammatory cytokines, which enhance the cytotoxicity of adaptive immune cells, thereby effectively suppressing the occurrence and progression of bacteria, viruses, and tumors [13–15]. Additionally, phosphorylated STING, when activated, has been reported to bind to the key glycolytic enzyme HK2, effectively inhibiting the Warburg effect and lactate secretion, which in turn suppresses tumorigenesis and progression [16]. However, the epigenetic and metabolic plasticity of tumors can suppress the expression of cGAS-STING pathway-related proteins within the tumor itself, mediating the formation of an immunosuppressive tumor microenvironment. Although demethylating agents like decitabine can reprogram the methylation of STING in glioma and promote STING expression, they cannot rule out the potential for non-specific inflammation in the central nervous system [17]. Therefore, strategies that can specifically mediate long-term activation of STING in glioma cells or efficiently reverse the immunosuppressive microenvironment could enhance the short-term survival rates of glioma patients in clinical settings.

Microenvironment-responsive tumor treatment strategies minimize damage to surrounding normal tissues and can be better applied in clinical translation [18]. Mesenchymal stem cell (MSC)-based drug delivery strategies have been shown to respond to the TGF-β signaling in the glioma microenvironment, efficiently homing to brain tumor sites, thus avoiding damage to normal central nervous tissue [19, 20]. Moreover, the cell membrane receptors of MSCs can effectively neutralize the immunosuppressive molecule TGF-β, further inhibiting the progression of glioma[21]. However, the in vivo differentiation pathways of MSCs are difficult to control, as they may potentially transform into tumor cells or differentiate into immunosuppressive cells, thereby promoting the rapid progression of glioma [22]. In recent years, exosomes secreted by MSCs have been reported to not only possess the tumor regulatory characteristics of their parent cells but also to deliver valuable cargo (such as proteins, lipids, RNA) through physiological barriers to target cells, playing a role in cell communication and regulation [23, 24]. They avoid the pitfalls of stem cells as vectors, becoming a new hotspot in cancer therapy.

Radiotherapy-mediated activation of STING protein has been reported to efficiently enrich activated STING protein in extracellular vesicles released by cells through a non-canonical autophagy pathway, allowing intercellular transmission and further activation of the STING pathway in downstream cells [25]. However, activated STING protein are degraded through the COPII vesicle-mediated autophagy pathway, reducing the duration of STING's action on downstream cells. The combined use of autophagy inhibitors can promote the retention of activated STING in the cytoplasm, enhancing the long-term release of downstream effector molecules such as type I interferons, thus effectively promoting anti-tumor immunity [26]. Additionally, immunogenic molecules derived from radiotherapy-induced intracellular molecules (damaged DNA, ROS, ATP, phosphatidylserine exposure, and mtDNA) are also secreted into small extracellular vesicles, endowing them with the ability to target innate immune cells [27–29]. These small extracellular vesicles can efficiently activate innate immune cells through the TLR signaling pathway and the cGAS-STING signaling pathway, effectively promoting the body's antitumor immune response.

In this study, we used radiotherapy-derived engineered stem cell exosomes as the drug carrier to load Braf1, a small molecule inhibitor of cellular autophagy activity. In order to enhance the content of activated STING in radiotherapy-derived stem cell exosomes (Rexo) and to efficiently target tumor cells in the tumor microenvironment, we over-expressed STING proteins and membrane-localized nanoantibody targeting the CD47 molecule [30]. The CD47 molecule has been reported to be highly expressed in glioma cells [31], and the targeting of the CD47 molecule by the nanobody can block the immunosuppressive signaling pathway of CD47/SIRPα, thus promoting the phagocytosis of tumor cells by macrophages/microglia, and further enhancing the natural immune effect.

This study showed that radiotherapy-derived engineered stem cell exosomes (BafA1@Rexo-SC) were enriched with high levels of phosphorylated STING proteins (pSTING) as well as a large mounts of anti-CD47 nanobody (nCD47) anchored to the cell membrane, and could load high amounts of the autophagy inhibitor BafA1. Compared with the normal MSCs derived exosomes, Rexo could be more effciently engulfed by M1/M2 macrophage or microglial, and simultaneously promote the release of pro-inflammatory factors such as TNF-α, IFN-α/β and chemokines associated with the promotion of tertiary lymphoid structure formation by activating the TLR signaling pathway and the cGAS-STING signaling pathway. When infused with BafA1@Rexo-SC (Rexo was enriched with activated pSTING, CD47 nanobody and the autophagy inhibitor braf1), the macrophages/microglial cells showed more pronounced activation of pro-inflammatory signaling pathways and was able to induce a significantly enhanced release of pro-inflammatory chemokines. In addition, intracranial injection of BafA1@Rexo-SC induced the formation

of more tertiary lymphoid structures in glioma regions while significantly promoting the production of stem cell-like $CD8^+$ T cells and exhausting precursor $CD8^+$ T cells compared to the other group. At the same time, glioma cells were able to take up more BafA1@Rexo-SC and promote the activation of their own cGAS-STING signaling pathway and the release of type I interferon in vitro and in vivo, which mediated the efficient phagocytosis of tumor cells by macrophages/microglia and the reversal of the immune-suppressive microenvironment, and ultimately enhanced the efficacy of immunotherapy (Scheme 1).

Results and discussion

The clinical correlations between STING expression and TLS formation

Overactivation of the cGAS protein promotes the formation of TLS, indirectly demonstrating the role of the cGAS-STING signaling pathway in inducing TLS generation [32]. However, the high methylation of the STING promoter region in the central nervous system limits the activation of STING, thereby suppressing the potential for TLS formation within the GME. This study aims to induce the formation of TLS by overloading activated STING proteins in the GME, thereby effectively promoting the occurrence of anti-tumor immunity. To validate the relationship between STING expression and TLS, we firstly explored the expression of STING at the transcriptional and translational levels in GBM patients. Compared to adjacent non-tumor tissues, Fig. 1A from the Cancer Genome Atlas (TCGA) database and Fig. 1B from the Clinical Proteomic Tumor Analysis Consortium (CPTAC) database show a phenomenon of high STING expression in the tumor region of GBM patients. This is primarily attributed to a large influx of immune cells highly expressing STING in GBM, rather than the glioma cells themselves [33]. To analyze the correlation between STING expression and TLS formation, we performed the data of single cell RNA sequencing analysis from the Chinese Glioma Patient Cancer Database (CGGA) and conducted unsupervised clustering analysis on immune cell subsets related to TLS formation [34]. The results shown in Fig. 1C, D revealed that in tumor regions with high STING expression, there is a more pronounced infiltration of T cells, B cells, and the generation of high endothelial venules. Moreover, chemokines associated with TLS formation were expressed in higher quantities in the GME with high STING expression (Fig. 1E), and their expression is mainly correlated with the infiltration of immune cells related to TLS formation (Fig. 1F). These results confirm a positive correlation between high STING expression in the GME and the infiltration of immune cells and secretion of chemokines associated with TLS formation.

Preparation and characterization of BafA1@Rexo-SC

Exogenous introduction of phosphorylated STING (pSTING) proteins into glioma cells and suppressive immune cells within the GME may reactivate the innate immune signaling pathways intrinsic to glioma. However, the metabolic half-life of activated pSTING in the cytoplasm is relatively short, primarily degraded through autophagy pathways. Inhibition of cellular autophagy levels can effectively suppress the degradation of pSTING, extending the activation duration of the cGAS-STING signaling pathway, thereby efficiently mediating the release of pro-inflammatory cytokines. Moreover, excessive inflammatory activation of the central nervous system may lead to the occurrence of neuroinflammation. Therefore, stem cell-derived exosomes with tumor-homing properties serve as the primary drug carrier candidates in this study. To better promote the phosphorylation of STING proteins and their accumulation within exosomes, we selected exosomes derived from stem cells post-radiotherapy (Rexo) as the drug carrier to deliver the autophagy inhibitor BafA1, as well as to automatically enrich pSTING and membrane-anchored nanobody targeting the CD47 molecule (nCD47). By highly targeting and regulating the anti-tumor functions of glioma cells and immunosuppressive cells within the GME, we aim to achieve efficient local tumor targeting and immune activation.

The acquisition strategy for BafA1@Rexo-SC (Rexo loaded with BafA1, pSTING and nCD47) is shown in Fig. 2A. To promote the accumulation of nCD47 in exosomes, we constructed nCD47 fusion proteins with membrane-anchored properties, the design of which is schematically shown in Fig. 2B**.** To localize the nCD47 to the surface of the cell membrane, a CD8α signal peptide sequence (MASPLTRFLSLNLLLLGESIILGSGEA) was added to the N-terminal of the nCD47 protein, and an EGFP sequence was added to the C-terminal of the nCD47 protein to allow tracing of the location of the nCD47. Meanwhile, a GPI membrane anchoring sequence (GGSSLQSTAGLLALSLSLLHLYC) was added at the end to anchor the nCD47 to the surface of the cell membrane. In addition, we constructed lentiviral plasmids that express both STING protein and membrane-anchored nCD47 proteins by using internal ribosome recognition sites, such as T2A peptide, and transfected the plasmid to bone marrow stem cell (MSCs). The confocal imaging in Fig. 2B showed that STING was predominantly distributed in the cytoplasm, whereas nCD47 was predominantly distributed at cell membrane sites. Dynamic light scattering, zeta potential and transmission

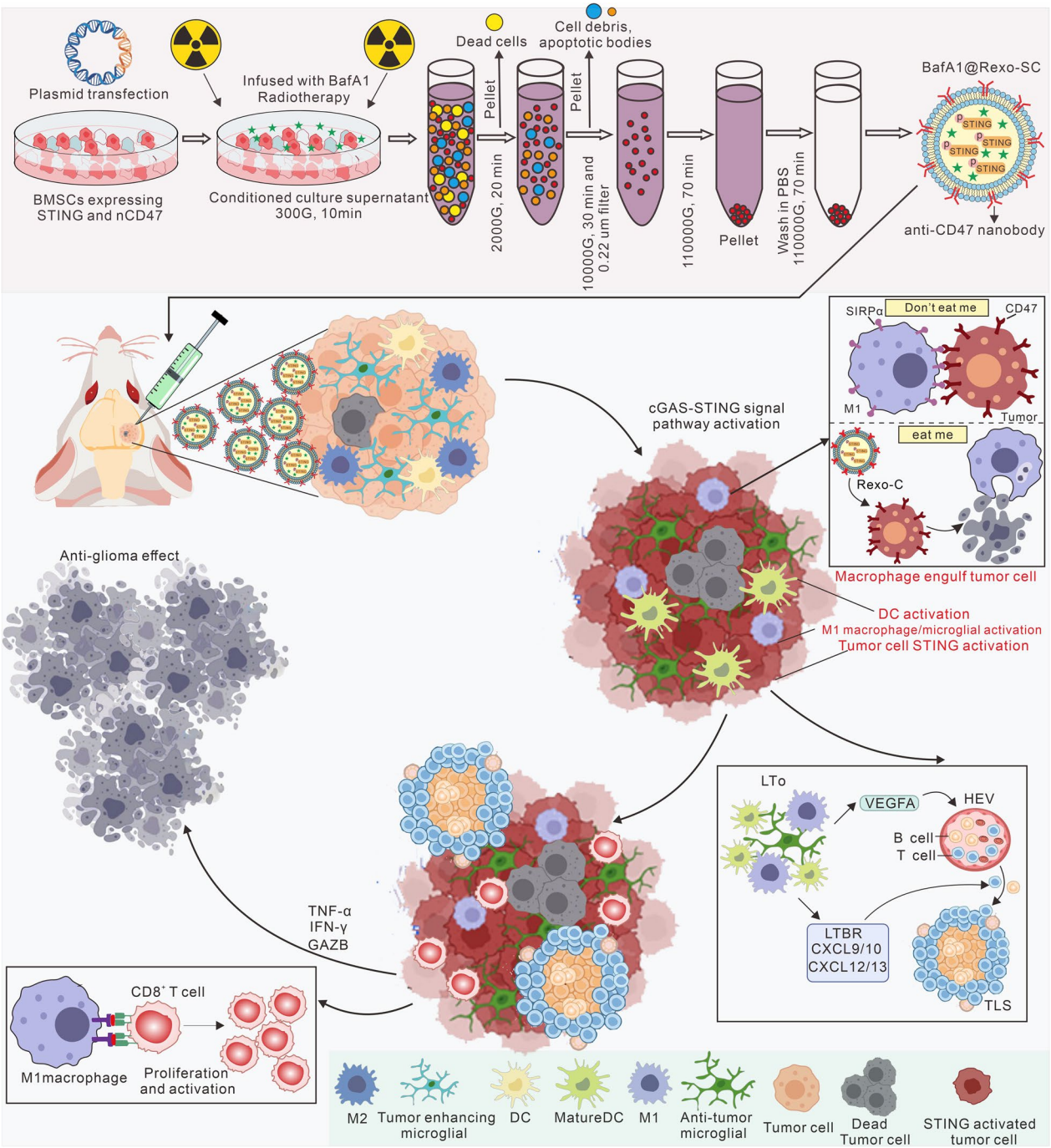

Scheme 1. The absence of signaling pathways related to intrinsic immune activation in tumor cells and the immunosuppressive microenvironment limit lymphocyte infiltration, constitutes an "immune-desert" tumor displaying insensitivity to various immunotherapies. This study constructed radiotherapy-derived engineered stem cell exosomes (BafA1@Rexo-SC) loaded with the autophagy inhibitor BafA1 expressing phosphorylated STING protein and membrane anchored anti-CD47 nanobody. Intracranial injection of BafA1@Rexo-SC could promote M1 polarization of infiltrating macrophages and microglial, phagocytosis of tumor cells by macrophages and antigen presenting cells, and activation of effector T cells. In addition, BafA1@Rexo-SC could also promote the release of a large amounts of cytokines associated with the formation of TLS and efficiently mediates the formation of TLS, ultimately reversing the tumor inhibitory immune microenvironment, and thus inhibiting the development of glioma cells

electron microscopy were used to identify the different engineered exosomes after radiotherapy (Fig. 2C–E). The particle size and zeta potential of exosomes, Rexo, Rexo-S (Rexo enriched for pSTING), Rexo-SC (Rexo enriched for pSTING and nCD47 fusion protein) and BafA1@Rexo-SC were essentially the same, predominantly distributed between 100 and 150 nm.

Meanwhile, western blotting experiment were used to identify whether target proteins were enriched in different engineered exosomes. The results in Fig. 2F showed that all engineered exosomes expressed classic exosomal marker proteins such as Alix, CD63, and CD81. The exosomes did not contain active pSTING or nCD47, whereas Rexo were enriched with some pSTING proteins. However, Rexo derived from MSCss overexpressing STING were highly enriched with pSTING proteins. The enrichment of nCD47 in Rexo did not affect the enrichment of pSTING. Furthermore, Rexo derived from MSCss overexpressing nCD47 were highly enriched with nCD47 fusion proteins, and the loading of the drug BafA1 did not affect the enrichment of pSTING and nCD47 fusion protein. We further investigated the release of BafA1 loaded in Rexo-SC in the presence of mouse serum using HPLC. A sustained release profile was observed (Fig. 2G), and after 72 h incubation, the concentration of BafA1 was about half of the original concentration, showing that Rexo-SC can release hydrophobic drugs such as BafA1. The above results confirmed that pSTING and nCD47 can be highly enriched in Rexo and had a strong loading capacity for BafA1.

Evaluation of the anti-tumor effect of BafA1@Rexo-SC on GL261 tumor cell

The low expression of STING protein in glioma cells limits the activation of innate immune signaling pathways, and enhancing the production of activated STING proteins in tumor cells can effectively promote the occurrence of antitumor immunity. MSCs have been reported to target and home to tumor sites. MSCs-derived exosomes, as primary mediators of cellular communication, also possess a certain degree of tumor targeting effect. However, it is unknown whether Rexo have an enhanced function in targeting glioma cells. Moreover, the highly expressed CD47 molecule on glioma cells can serve as one of the effective targets for targeting glioma cells, and by simultaneously blocking the CD47-SIRPα signaling axis [35], it may further enhance the phagocytic effect of macrophages on glioma cells.

To compare the targeting properties of engineered exosomes with different functional components on GL261 tumor cells, we co-incubated the indicated engineered exosomes labeled with PKH26 dye with GL261 cells for 24 h. Subsequently, we identified the targeting characteristics of the various engineered exosomes using laser confocal microscopy (Fig. 3A) and flow cytometry (Fig. 3B, C). The results in Fig. 3A demonstrated that GL261 highly expresses the CD47 molecule, and the targeting of exosomes to GL261 was relatively weak. In contrast, Rexo significantly enhance the targeting properties towards GL261, likely due to the radiotherapy-mediated enrichment of immunogenic molecules in Rexo, which increases the non-specific uptake of Rexo by GL261 cells. Moreover, Rexo-C, which was enriched with nCD47, exhibited a more pronounced targeting characteristic towards GL261 compared to Rexo, confirming that targeting the CD47 molecule promotes the uptake of Rexo by GL261. Additionally, the results in Fig. 3C confirm that Rexo-S or Rexo-SC, enriched with pSTING, didn't affect the targeting of Rexo or Rexo-C to tumor cells, and BafA1 does not influence the targeting characteristics of Rexo-SC towards GL261. These experimental results confirm that radiotherapy in combination with nCD47 targeting can synergistically enhance the efficient targeting properties of engineered exosomes towards GL261.

The activation of NF-κB by Toll-like receptor (TLR) signaling pathways and the activation of the cGAS-STING pathway have both been demonstrated to efficiently mediate the release of cytokines associated with the formation of tertiary lymphoid structures (TLS). Radiotherapy-derived microparticles have been reported to possess strong immunogenicity and to efficiently activate the NF-κB pathway in effector cells, promoting the release of TNF-α from target cells. In this study, we aim to utilize BafA1@Rexo-SC to simultaneously activate the NF-κB and cGAS-STING signaling pathways in target cells, thereby efficiently promoting the release

(See figure on next page.)

Fig. 1 Identification of clinical correlations between STING1 expression and TLS formation. **A** Identify the expression of STING1 (TMEM173) gene between tumors and adjacent cancer in the TCGA database. **B** Identify the expression of STING1 protein between tumor patients and normal samples in the Clinical Proteomic Tumor Analysis Consortium (CPTAC) database. **C** Distribution of cells associated with TLS formation in patients with high and low STING expression (The single cell RNA sequencing data from Chinese Glioma Genome Atlas (CGGA) database). **D** Differences in the relative number of cells associated with TLS formation in patients with high and low STING expression. **E** Differential expression of cytokines associated with TLS formation in GBM patients with high and low STING expression. **F** Distribution of expression of cytokines associated with TLS formation in different cells in GBM patients with high STING expression

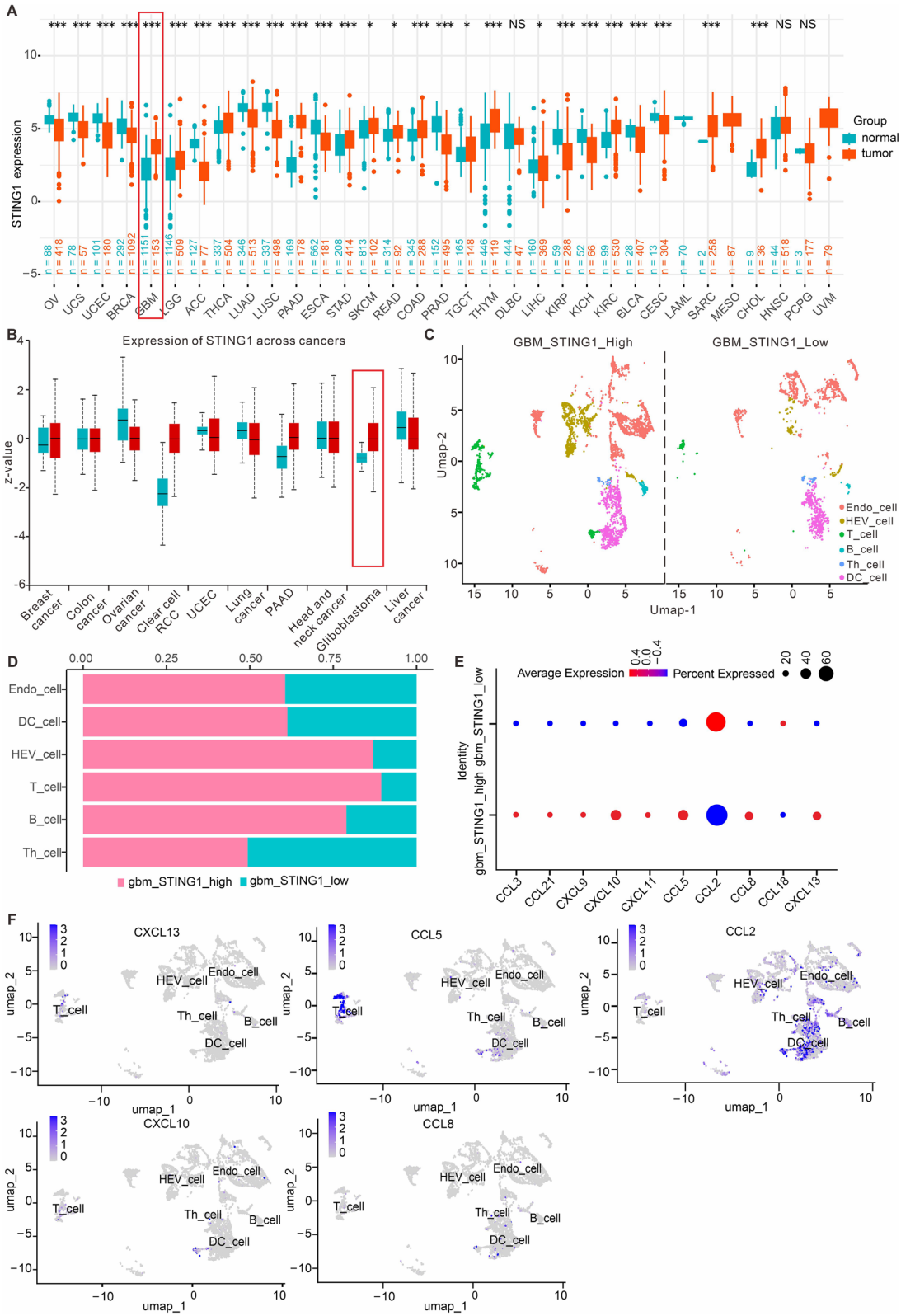

Fig. 1 (See legend on previous page.)

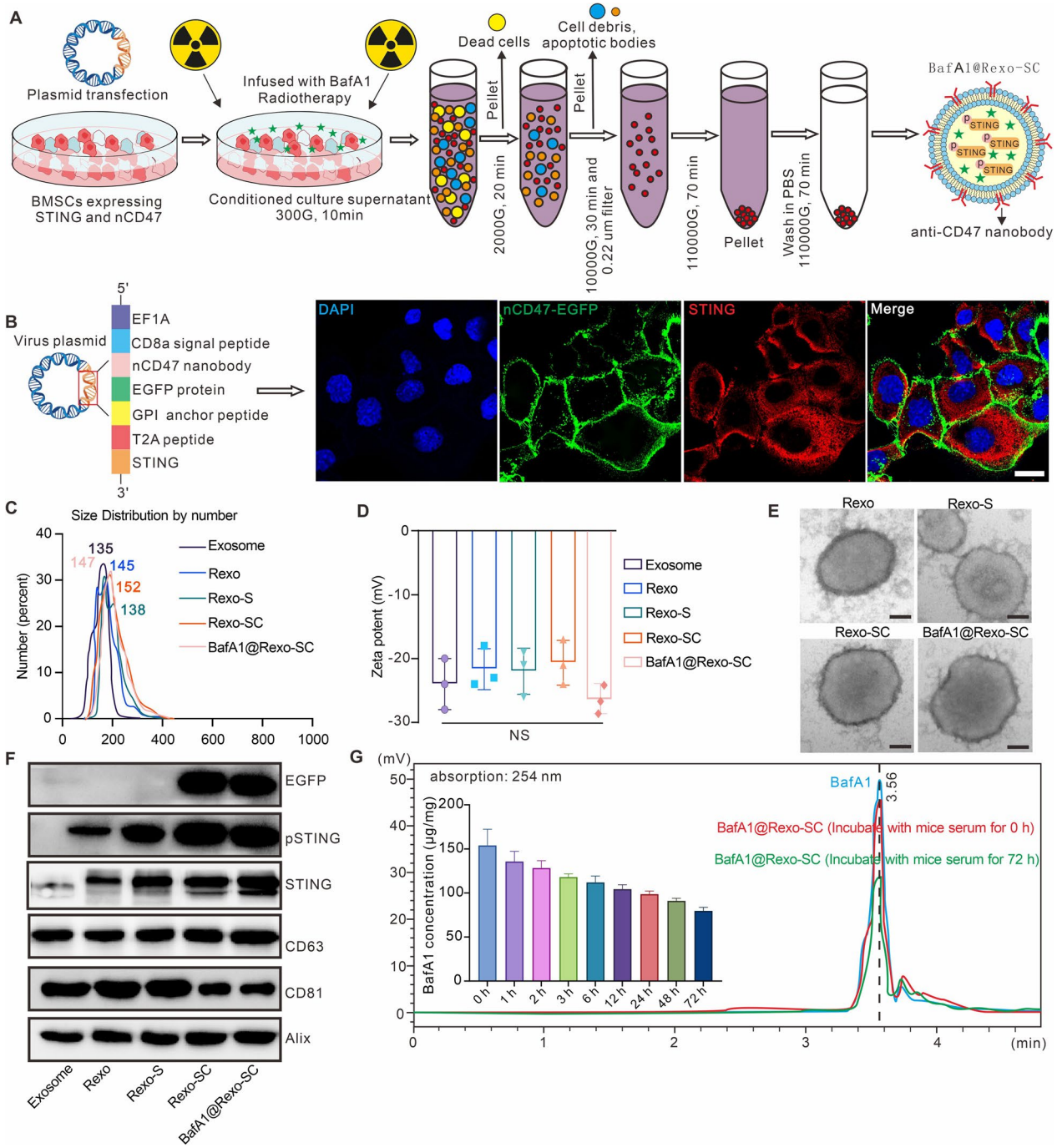

Fig. 2 Preparation and characterization of BafA1@Rexo-SC. **A** Schematic of BafA1@Rexo-SC preparation. **B** Schematic diagram of a plasmid constructed to express both membrane-anchored anti-CD47 nanobodies and STING proteins, and the representative images for the location of anti-CD47 nanobodies and STING proteins in mouse bone marrow-derived stem cells (MSCss) by confocal imaging, scale bar: 10 μm. **C** Size distribution of different engineered exosomes measured by dynamic light scattering. **D** Zeta potential of different engineered exosomes measured by Malvern laser particle size analyzer. **E** Size distribution of different engineered exosomes measured by transmission electron microscopy, scale bar: 50 nm. **F** Analysis of the expression of Alix, CD81, CD63, STING, Phosphorylating STING (pSTING) and EGFP in different engineered exosomes by using western blotting experiment. **G** HPLC to be used to identify the drug release characteristics of BafA1@Rexo-SC. Data are presented as the mean ± SD. $^{*}P < 0.05$, $^{**}P < 0.01$, $^{***}P < 0.001$, and NS: not significant

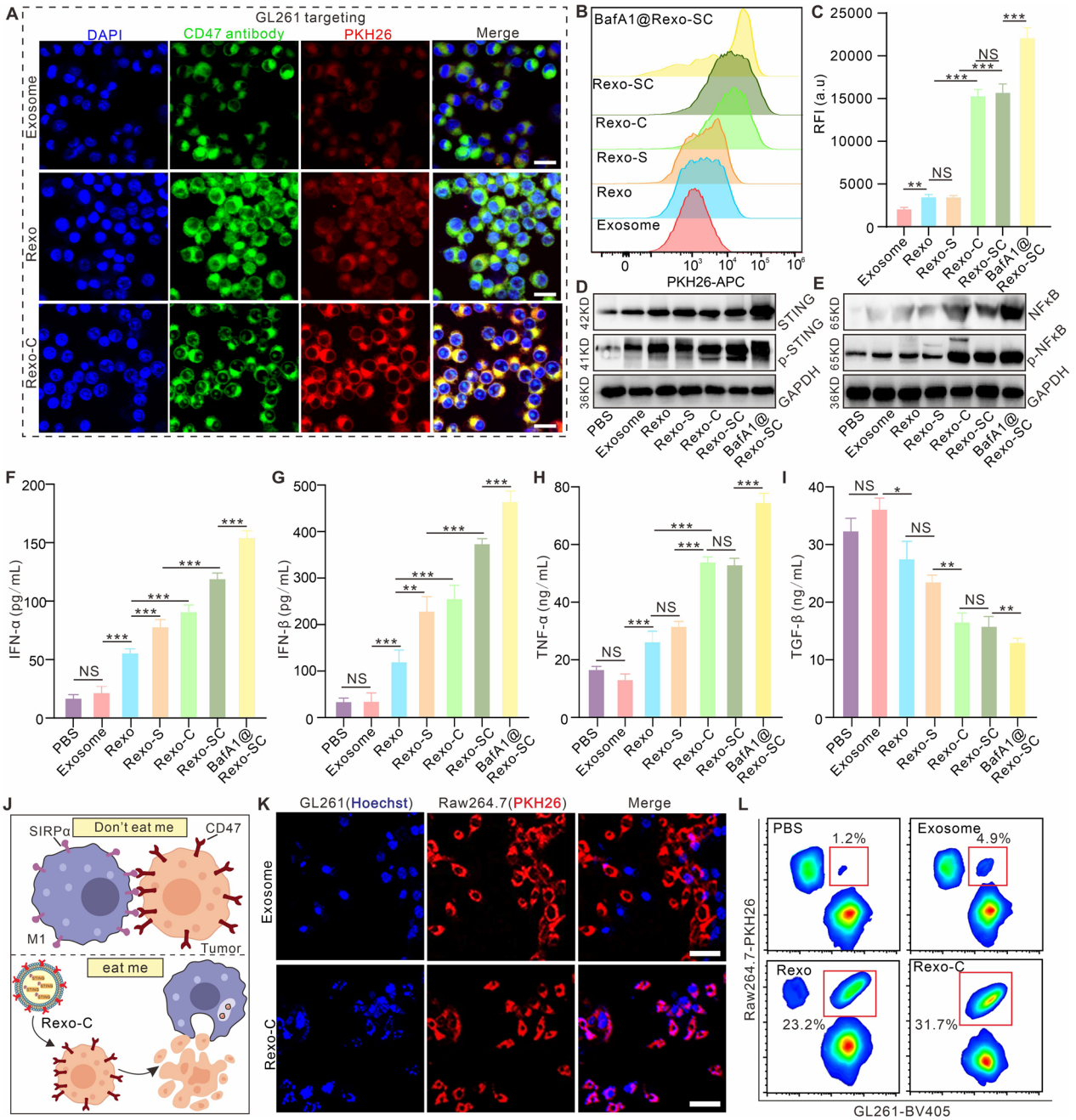

Fig. 3 Evaluation of BafA1@Rexo-SC targeting effects on GL261, activation effect of endogenous immune signaling pathways, and shielding properties of CD47-SIRPα signaling. **A** Representative images of different engineered exosomes uptake in GL261 tumor cells obtained by confocal imaging. Nuclei were labeled using DAPI (blue), Rexo or Exosome were pre-labeled using PKH26 dye (red), and GL261-expressed CD47 molecules were labeled using Alexfluo647-labeled CD47 antibody (green). The scale bar is 20 μm. **B**, **C** Analysis and statistics of the targeting properties of different engineered exosomes on GL261 tumor cells by flow cytometry. **D** Analysis of the expression of STING and pSTING in GL261 tumor cells after incubation with different engineered exosomes for 24 h by using western blotting experiment. **E** Analysis of the expression of NF-κB and pNF-κB in GL261 tumor cells after incubation with different engineered exosomes for 24 h by using western blotting experiment. **F**–**I** Detection of IFN-α (**F**), IFN-β (**G**), TNF-α (**H**) and TGF-β (**I**) in the supernatants of GL261 cells incubated with different engineered exosomes for 24 h by using Elisa kit. **J** Illustration of how Rexo-C influence macrophage phagocytosis of tumor cells. **K** Confocal microscopy to evaluate the enhancement of glioma cell phagocytosis by macrophages due to Rexo-C infusion, with a scale bar of 50 μm. The nuclei of GL261 cell was labeled with Hoechst (blue) and the membrane of RAW264.7 cell was labeled with PKH26 (Red). **L** Comparative flow cytometry to assess the promotion of tumor cell uptake by macrophages using different engineered exosomes. Data are presented as the mean ± SD. **P* < 0.05,***P* < 0.01, ****P* < 0.001, and NS: not significant

of pro-inflammatory cytokines and cytokines related to TLS formation. As Rexo-SC has been proven to efficiently target GL261 cells, we subsequently validated whether BafA1@Rexo-SC could mediate the activation of the cGAS-STING and NF-κB signaling pathway in target cells. Compared to GL261 cells incubated with Rexo, the results of western blotting experiments depicted in Figs. 3D, E and S1 (Supporting imformation) revealed significant differences in the activation of STING protein and NF-κB protein in GL261 cells incubated with Rexo-C and Rexo-S. Furthermore, Rexo-SC was able to further promote the activation of STING and NF-κB proteins, while BafA1@Rexo-SC was able to maximize the mediation of STING protein activation and NF-KB protein activation. The primary reason for this was that BafA1 could inhibit the lysosomal degradation of pSTING and phosphorylated NF-κB (pNF-κB), thereby enhancing their residence time in the cytoplasm. Additionally, we employed an enzyme-linked immunosorbent assay (ELISA) to assess the release of pro-inflammatory and anti-inflammatory cytokines in the supernatant of GL261 cells incubated with different engineered exosomes. The statistical results in Figs. 3F, G confirmed that the concentrations of cytokines such as IFN-α and IFN-β in the supernatant were correlated with the degree of STING protein activation in GL261 cells, with BafA1@Rexo-SC mediating the highest level of type I interferon release. Meanwhile, the statistical results in Fig. 3H confirmed that the concentration of TNF-α in the supernatant was directly proportional to the activation degree of the NF-κB signaling pathway in GL261 cells, with BafA1@Rexo-SC mediating the highest level of TNF-α release. We also verified the secretion of anti-inflammatory cytokines such as TGF-β in the supernatant of GL261 cells incubated with different engineered exosomes (Fig. 3I). Compared to the PBS group, exosomes didn't inhibit the secretion of TGF-β by GL261 cells, while other indicated engineered exosomes significantly suppressed TGF-β secretion, with BafA1@Rexo-SC exhibiting the highest degree of inhibition, showing a significant difference from other groups. The aforementioned experimental results confirm that BafA1@Rexo-SC can efficiently activate the cGAS-STING signaling pathway and the NF-κB signaling pathway in GL261 cells, effectively promoting the release of pro-inflammatory cytokines and inhibiting the release of anti-inflammatory cytokines.

In addition to promoting the uptake of Rexo by GL261 cells, nCD47 was also able to efficiently shield the CD47-SIRPα signaling pathway, thereby effectively promoting the uptake of tumor cells by macrophages. Here, we also verified whether Rexo enriched with nCD47 could promote the uptake of GL261 by LPS activated RAW264.7 (Fig. 3J). The confocal imaging results presented in Figs. 3K and S2 (Supporting imformation) demonstrate that GL261 cells pre-incubated with Rexo-C were more readily engulfed by Raw264.7 macrophages compared to those incubated with exosomes, which were seldom ingested by Raw264.7 cells. We further quantified the phagocytosis of GL261 cells by macrophages after co-incubation with exosomes, Rexo, or Rexo-C using flow cytometry. The results in Fig. 3L reveal that Rexo could to some extent facilitate the uptake of GL261 by RAW264.7, primarily due to the immunogenic molecules it carries, which enhance the recognition of GL261 by RAW264.7 cells. Moreover, Rexo-C loaded with nCD47 further mediated the uptake of GL261 by RAW264.7 cells, confirming the efficacy of nCD47 in promoting phagocytosis.

Evaluation of BafA1@Rexo-SC targeting effects and activation effect on BMDC and BMDM

The immunosuppressive microenvironment is an extrinsic factor contributing to the resistance of GBM to immunotherapy, primarily comprising a substantial infiltration of M2-type macrophages, tumor-promoting microglia, and tolerogenic dendritic cells (DCs) [36]. The cGAS-STING signaling pathway is pivotal in mediating the antitumor effects of innate immune cells. Therefore, we proceeded to investigate whether BafA1@Rexo-SC could target and activate antigen-presenting cells (APCs) and phagocytic cells.

As shown in Figs. 4A, F for confocal imaging results, exosomes demonstrated weaker targeting of BMDM and BMDC after co-incubation with GL261 cells for 24 h, whereas Rexo demonstrated excellent targeting of both types of cells. The statistics of fluorescence intensity for BMDC (Fig. 4B, C) and BMDM (Fig. 4G, H) uptake also showed results consistent with confocal imaging. In addition, the enrichment of pSTING as well as nCD47 in Rexo had no significant effect on its properties in targeting BMDM or BMDC, whereas BafA1, although significantly enhancing the fluorescence intensity of BMDM or BMDC, was mainly related to the inhibition of lysosomal degradation of the dye.

We simultaneously explored the activation effects of BafA1@Rexo-SC on BMDC and its reprogramming effects on M2-type BMDM. Statistical analysis of the expression levels of CD86 (Fig. 4E) and MHC-II (Fig. 4F) in BMDC incubated with indicated treatments at equivalent protein concentration revealed that exosomes alone had no regulatory effect on the functions of BMDC and BMDM. In contrast, Rexo significantly enhanced the expression of CD86 and MHC-II in BMDC while markedly reducing the expression of CD206 in M2 macrophages. Furthermore, as the accumulation of pSTING in target cells increased, the Rexo-S and Rexo-SC group further enhanced the expression of CD86 and MHC-II

in BMDC, achieving expression levels twice that of the Rexo group, and further reduced CD206 expression in M2 type BMDM to two-thirds of that seen in the Rexo group (Fig. 4I). Additionally, the inhibition of autophagic activity by BafA1@Rexo-SC promoted the retention of pSTING in the cytoplasm, further enhancing the expression of CD86 and MHC-II in BMDC to 1.5 times that of the Rexo-S group, while the expression of CD206 in M2 type BMDM co-incubated with BafA1@Rexo-SC was half that of the Rexo-SC group. These results demonstrate that BafA1@Rexo-SC can efficiently mediate the activation of dendritic cells and the reprogramming of M2-type macrophages.

To further validate the efficacy of BafA1@Rexo-SC, we assessed the secretion of type I interferons associated with the activation of the cGAS-STING signaling pathway and TNF-α cytokines linked to the activation of the NF-κB signaling pathway. Statistical analysis of the concentrations of type I interferons and TNF-α in the supernatants of BMDC and BMDM co-incubated with indicated treatments at equivalent protein concentrations (Fig. 4J–L) showed that with the enhanced phagocytosis of the indicated treatments by BMDM and BMDC, as well as the increased accumulation of pSTING in these two cell types, the release of type I interferons and TNF-α also progressively increased. Notably, the most pronounced enhancement was observed in the BafA1@Rexo-SC group, confirming its potential to initiate innate immune activity.

Evaluate the ability of BafA1@Rexo-SC to induce release of cytokines associated with tertiary lymphoid structure formation from BMDC and BMDM in vitro

TLR agonist-activated macrophage/microglials have been reported to act as "Lto" cells for initiating the generation of tertiary lymphoid structures, and here we also explored whether BafA1@Rexo-SC could promote the release of cytokines associated with tertiary lymphoid structures by DCs, macrophages, or microglia. RNA-seq was performed to investigate the effects of BafA1@Rexo-SC on gene expression and signaling pathways in M2 type BMDM. The results showed 1232 DEGs in BMDM after treatment with BafA1@Rexo-SC (Fig. 5A). Subsequent bioinformatic analysis revealed that the cytosolic DNA-sensing pathway, TNF signaling pathway, NF-κB signaling pathway was enriched in BMDM (Fig. 5B, C), which was consistent with the results described in previous experiments. In addition, the result in Fig. 5B also showed that the signaling pathways associated with the formation of tertiary lymphoid structures was enriched in BMDM, such as leukocyte migration, myeloid leucocyte migration and cytokine-cytokine receptor interaction. Compared to other indicated treatment group, the expression of genes related to the formation of tertiary lymphoid structures significantly increased in BafA1@Rexo-SC group (Fig. 5D). Growth factor VEGFA that promotes high endothelial microvessel generation and chemokines CXCL9 or CXCL10 that promotes the formation of tertiary lymphoid structure in the cell culture supernatants of BMDC, BMDM and BV2 were also increased most significantly in the BafA1@Rexo-SC group (Fig. 5E, G, H). In addition, LTBR, which interacts with Lta/b in "lymphoid tissue inducer cells (Lti)" cells, was also significantly highly expressed in natural immune cells co-incubated with BafA1@Rexo-SC (Fig. 5F). In contrast, GL261 cells co-incubated with different indicated treatments expressed low amounts of VEGFA, were largely devoid of LTBR and released associated chemokines. In conclusion, BafA1@Rexo-SC has the potential to target and promote the secretion of cytokines associated with tertiary lymphoid structure formation by natural immune cells in vitro.

Evaluation of the targeting properties of BafA1@Rexo-SC on tumor cells and GBM related immune cells in vivo

Rexo containing pSTING or BafA1 does not affect Rexo targeting, whereas Rexo containing nCD47 affects its tumor cell targeting properties. Therefore, we mainly explored the targeting of exosome, Rexo, and Rexo-C to tumor cells themselves and to immune cells in the GME

(See figure on next page.)

Fig. 4 Evaluation of BafA1@Rexo-SC targeting effects and activation effect on BMDC and BMDM. **A** Representative images of different engineered exosomes uptake in BMDC obtained by confocal imaging. Nuclei were labeled using DAPI (blue), Rexo or Exosome were pre-labeled using PKH26 dye (red), and the cell membrane wwa labeled using PKH67 (green). The scale bar is 20 μm. **B**, **C** Analysis and statistics of the targeting properties of different engineered exosomes on BMDC by flow cytometry. **D** Analysis and statistics of CD86 expression of BMDC after incubated with different engineered exosomes for 24 h by flow cytometry. **E** Analysis and statistics of MHC-II expression of BMDC after incubated with different engineered exosomes for 24 h by flow cytometry. **F** Representative images of different engineered exosomes uptake in BMDM (M2 type) obtained by confocal imaging. Nuclei were labeled using DAPI (blue), Rexo or Exosome were pre-labeled using PKH26 dye (red), and the cell membrane was labeled using PKH67 (green). The scale bar is 20 μm. **G**, **H** Analysis and statistics of the targeting properties of different engineered exosomes on BMDM by flow cytometry. **I** Analysis and statistics of CD206 expression of BMDM after incubated with different engineered exosomes for 24 h by flow cytometry. **J**–**L** Detection of IFN-α (**J**), IFN-β (**K**) and TNF-α (**L**) in the supernatants of BMDC and BMDM incubated with different engineered exosomes for 24 h by using Elisa kit. Data are presented as the mean ± SD. *$P < 0.05$,**$P < 0.01$, ***$P < 0.001$, and NS: not significant

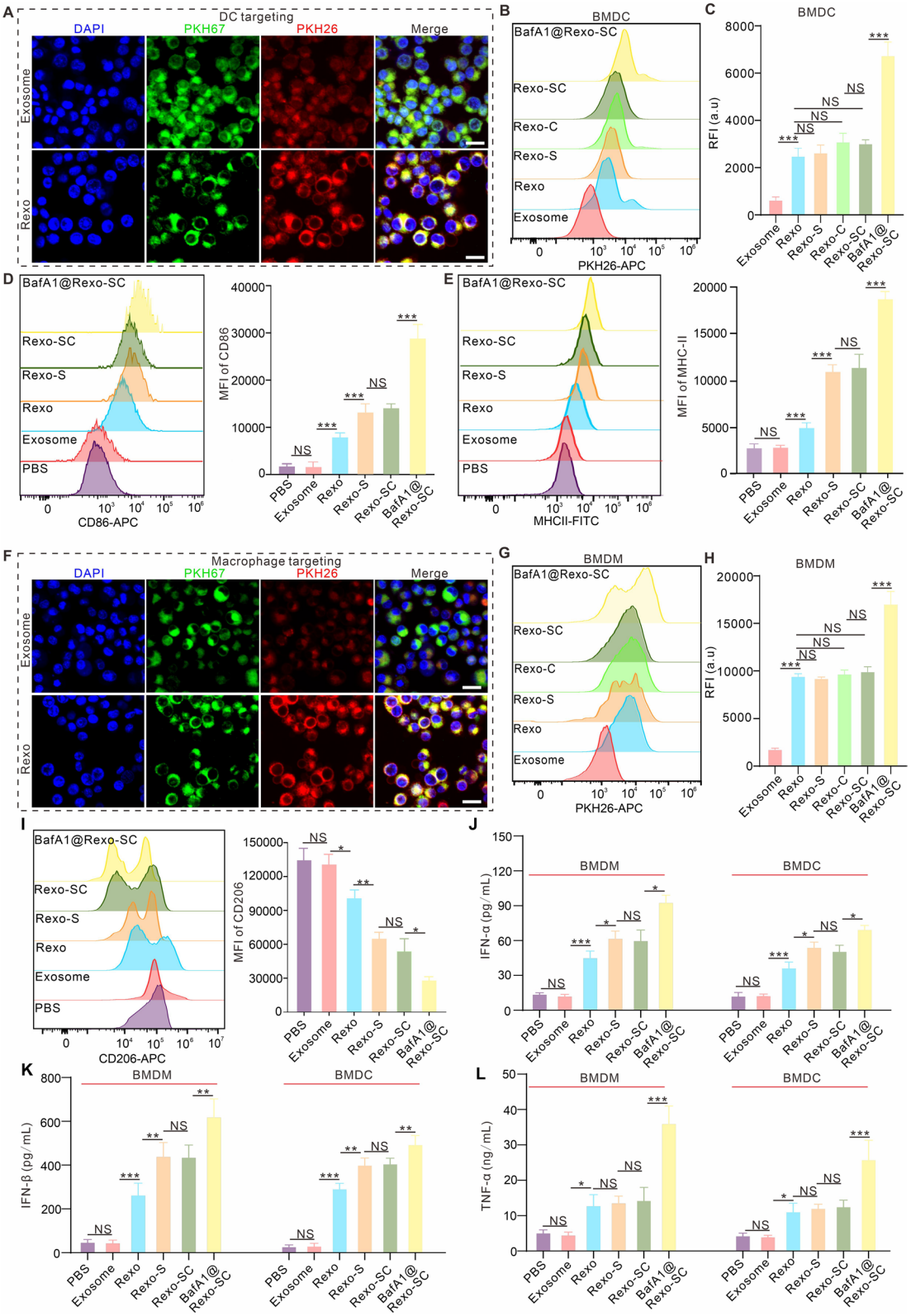

Fig. 4 (See legend on previous page.)

in vivo. To explore the tissue distribution of different exosomes *in vivo*, we performed intracranial injections of 50 μg PKH26-labelled exosome, Rexo, or Rexo-C (5 μL) into mice previously implanted with GL261-mcherry cells. 24 h later, the mice were sacrifced and part of the tumor were dispersed to generate a single cell suspension for fow cytometry analysis and part of the tumor were made into frozen sections for immunofluorescence experiments. A schematic diagram of the relevant study is shown in Fig. 6A. There were significant differences in the percentages of PKH26-positive tumor cells, T cells,

B cells, neutrophils, DCs, or M2 macrophages between mice injected with exosomes, Rexo or Rexo-C (Fig. 6B). Exosomes predominantly targeted tumor cells and had lower targeting properties for other immune cells, whereas Rexo significantly enhanced the targeting of GME immune cells, and the targeting of tumor cells was not significantly different from that of exosomes. Rexo-C containing nCD47 predominantly enhanced the targeting of tumor cells, whereas the targeting of immune cells was not significantly different from that of Rexo. Tumor sections were stained using antibodies targeting DCs, and macrophages. The results confrmed that Rexo and Rexo-C could be efficiently taken up by the relevant immune cells, and Rexo-C could also be engulfed by GL261-mcherry tumor cells (Fig. 6C, D).

In vivo *validation of the therapeutic potential and TLS formation ability of BafA1@Rexo-SC against glioma*

The previous results have confirmed the successful construction of BafA1@Rexo-SC and its efficient targeting of tumor cells and natural immune cells and effective regulation of signaling pathways related to immune activation. To evaluate if BafA1@Rexo-SC could control the growth of glioma in vivo, we established a mouse glioma model using GL261-luciferase (GL261-Luc) cells, following the treatment protocol depicted in Fig. 7A. Different mouse groups underwent in vivo small animal imaging. The data in Fig. 7B indicate that all engineered Rexo except exosomes demonstrated therapeutic effects on glioma model. Especially, the group receiving BafA1@Rexo-SC displayed the most significant growth inhibition. Compared to the survival rates of mice in the PBS group and the exosomes group at 22 days, survival analysis (Fig. 7C) and body weight changes across different groups (Fig. 7D) indicate that the Rexo group significantly prolongs the survival of mice to 30 days. Furthermore, Rexo-S and Rexo-SC, which contain pSTING and nCD47, extend the survival of mice to approximately 40 days. Notably, BafA1@Rexo-SC promoted complete tumor remission in 20% of the tumor-bearing mice.

To verify whether the favorable therapeutic effects of BafA1@Rexo-SC are associated with the formation of tertiary lymphoid structures (TLS), we performed immunofluorescence on tumor samples from mice treated with indicated treatment to observe the formation of high endothelial venules (HEV) and TLS within the tumor area [37]. Confocal imaging results in Fig. 7E revealed that all groups had a significant presence of $CD31^+$ vascular endothelial cells in the tumor area. However, the PBS group and the exosomes group showed negligible MECA-79^+ HEV-associated endothelial cells. As the accumulation of pSTING in the GME increased, there was a concomitant increase in MECA-79^+ HEV-associated endothelial cells, with the BafA1@Rexo-SC group exhibiting the most pronounced generation of HEVs and co-localization with $CD31^+$ vascular endothelial cells. Additionally, the results in Fig. 7F confirmed that both the BafA1@Rexo-SC group and the Rexo-SC group contained TLS formed by $CD4^+$ T cells and B cells, with this phenomenon being more pronounced in the BafA1@Rexo-SC group. Although Rexo-S and Rexo could induce substantial infiltration of $CD4^+$ T cells and B cells, they failed to form effective TLS, likely due to insufficient secretion of cytokines related to TLS formation. Collectively, these findings verify that BafA1@Rexo-SC can effectively regulate the infiltration of T and B cells and the formation of tertiary lymphoid structures, and can achieve a certain probability of complete cure in tumor-bearing mice.

(See figure on next page.)

Fig. 5 Assessment of the ability of BafA1@Rexo-SC induced release of cytokines associated with tertiary lymphoid structure formation from BMDC and BMDM in vitro. **A** Volcano plot of differentially expressed genes in the PBS group and the BafA1@Rexo-SC group of M2 type BMDM after co-incubation for 24 h. **B** Bubble chart of signaling pathways affected by BafA1@Rexo-SC in M2 type BMDM according to KEGG pathway enrichment analysis. **C** GSEA of the cytosolic DNA-sensing pathway. **D** Heatmaps showing up-regulated expression of genes associated with TLS formation in the indicated treatment group of M2 type BMDM. (**E**–**H**) Detection of the expression of cytokines associated with the formation of tertiary lymphoid structures [VEGFA (**E**), CXCL9 (**G**) and CXCL10 (**H**)] in the supernatants of BMDC, BV2, GL261 and BMDM incubated with different engineered exosomes for 24 h by using Elisa kit, and the surface receptors LTβR associated with the formation of tertiary lymphoid structures on the BMDC, BV2, GL261 and BMDM (**F**) by using flow cytometry. Data are presented as the mean ± SD. *$P < 0.05$,**$P < 0.01$, ***$P < 0.001$, and *NS* not significant

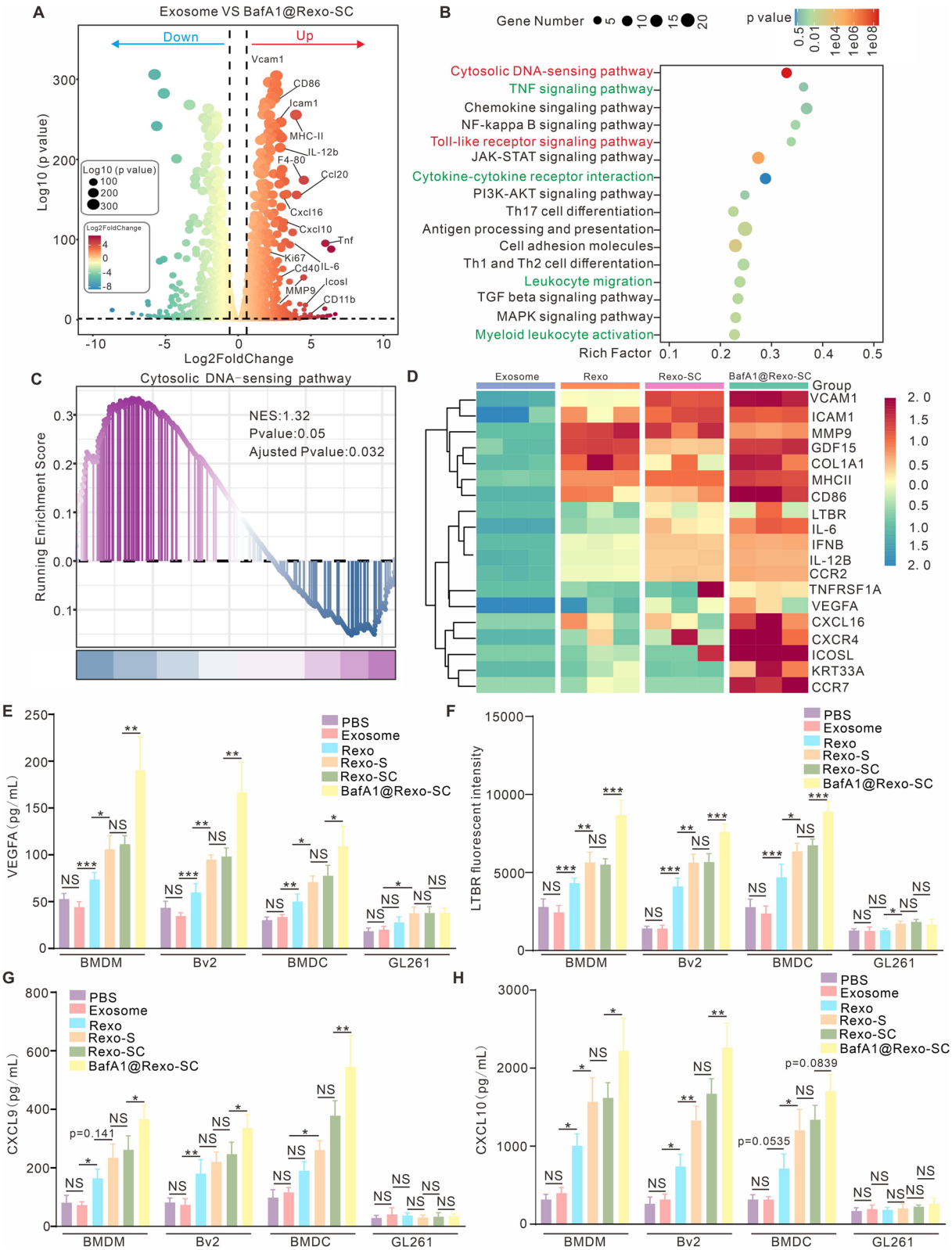

Fig. 5 (See legend on previous page.)

Validation of the ability of BafA1@Rexo-SC to reverse the GME

Injection of BafA1@Rexo-SC have effectively inhibited the in-situ growth of GL261 and significantly enhanced the formation of HEV and TLS in GL261 tumor area. We subsequently investigated the effects of BafA1@Rexo-SC on the infiltration of immune cells associated with the formation of TLS and the release of cytokines related to TLS formation. Additionally, we explored the release of pro-inflammatory cytokines that mediate the occurrence of antitumor immunity. Flow cytometry results indicated that the injection of BafA1@Rexo-SC led to a notable increase in the number of B cells ($CD45^+B220^+$), the number of activated DCs ($CD45^+CD11c^+CD86^+MHC\text{-}II^+$) and the number of effector $CD8^+$ T cells ($CD45^+CD3^+CD8^+IFN\text{-}\gamma^+$) within the GME (Fig. 8A, B, D). Additionally, compared to the PBS group and the exosomes group, Rexo significantly reduced the proportion of M2-type macrophages/microglia in the GME (Fig. 8C). With the increased presence of pSTING in the GME, the proportion of M2-type macrophages/microglia was further decreased. Notably, BafA1@Rexo-SC, compared to other groups, was able to most effectively reduce the proportion of M2-type macrophages/microglia. Consistent with these findings, BafA1@Rexo-SC induced the highest degree of pro-inflammatory cytokine release in the GME, including Type I and Type II interferons as well as tumor necrosis factor-alpha (TNF-α) (Fig. 8I, J). These data reveal that BafA1@Rexo-SC can effectively reverse the suppressive immune microenvironment and promote the onset of cellular immunity.

Provided that TLSs effectively promoted the infiltration of memory T cells and naive T cells in the tumor area [38], we conducted further analysis of the immune cells related to the formation of TLS within GME. The infiltration of central memory T cells ($CD8^+CD44^+CD62L^+$), exhausting precursor T cells ($CD3^+CD8^+TCF\text{-}1^+PD\text{-}1^-$) and naive $CD4^+/CD8^+$ T cells were significantly increased in BafA1@Rexo-SC group (Fig. 8E–H). Besides, These findings aligned with the characteristic immunological features of TLS formation. In addition, we also examined the expression of chemokine and growth factor associated with the formation of TLS using a custom multi-cytokine assay kit. Figure 8K–O demonstrated that, compared to other groups, the growth factor VEGFA and the chemokine such as CXCL9, CXCL10, CXCL12 and CXCL13 were significantly upregulated in the supernatant from the glioma mouse model injected with BafA1@Rexo-SC. These rusults showed that BafA1@Rexo-SChas the potential to induce the generation of tertiary lymphoid structures.

To confirm nCD47 induced phagocytosis of tumor cells by macrophage and DCs in vivo, immunofluorescence on glioma models injected with indicated treatment was performed. Figure 8P, Q illustrated that in the BafA1@Rexo-SC or Rexo-SC injected group, macrophage (marked in green) and DCs (marked in yellow) effectively engulfed GL261 tumor cells (marked in red), unlike macrophage and DCs in the Rexo or exosomes injected group. In addition, Fig. 8Q demonstrated that DCs in the BafA1@Rexo-SC or Rexo-SC group that had uptaken tumor cells were able to communicate with $CD8^+$ T cells (marked in green), and that this communication was more intimate in BafA1@Rexo-SC group, proving the in vivo phagocytosis-inducing uptake of tumor cells and activation effect on effector T cells by injection of BafA1@Rexo-SC. These results confirm that BafA1@Rexo-SC plays a crucial role in modulating the GME and induce the formation of TLS, which offers a novel therapeutic approach for the clinical treatment of GBM patients.

Conclusion

The present study presents a groundbreaking approach to enhancing immunotherapy for GBM by developing radiotherapy-derived engineered stem cell exosomes, termed BafA1@Rexo-SC. These exosomes are engineered to overexpress nCD47 and pSTING, and are loaded with the autophagy inhibitor BafA1, offering a multifaceted strategy to combat the immunosuppressive glioma microenvironment.

Our findings demonstrate that BafA1@Rexo-SC effectively targets tumor cells and immune cells within the GME, leading to the activation of antigen-presenting cells, macrophage/microglia polarization, and the formation of TLS. The activation of the cGAS-STING

(See figure on next page.)

Fig. 6 Different engineered exosomes accumulated in tumor cells and different subsets of immunocytes in tumor tissue in vivo. **A** Experimental plan: Female C57BL/6 mice, aged 6 weeks were used to establish intracranial GBM model. Glioma-bearing mice (GL261-mcherry) were injected intracranially (i.c.) with 5 μL of different engineered exosomes carrying the PKH26 dye on day 7. The glioma-bearing brain sample were collected at day 8, following with flow cytometry and immunofluorescence staining. **B** Quantization of exosomes, Rexo and Rexo-C accumulation in tumor cells and distinct immunocytes in tumor. **C** Immunofluorescence staining assay to identify the in vivo targeting ability of exosomes and Rexo to DC cells, the scale bar is 100 μm. **D** Immunofluorescence staining assay to identify the in vivo targeting ability of exosomes and Rexo to macrophages/microglial and tumor cells, the scale bar is 200 μm. Data are presented as the mean ± SD. $^*P < 0.05$,$^{**}P < 0.01$, $^{***}P < 0.001$, and *NS* not significant

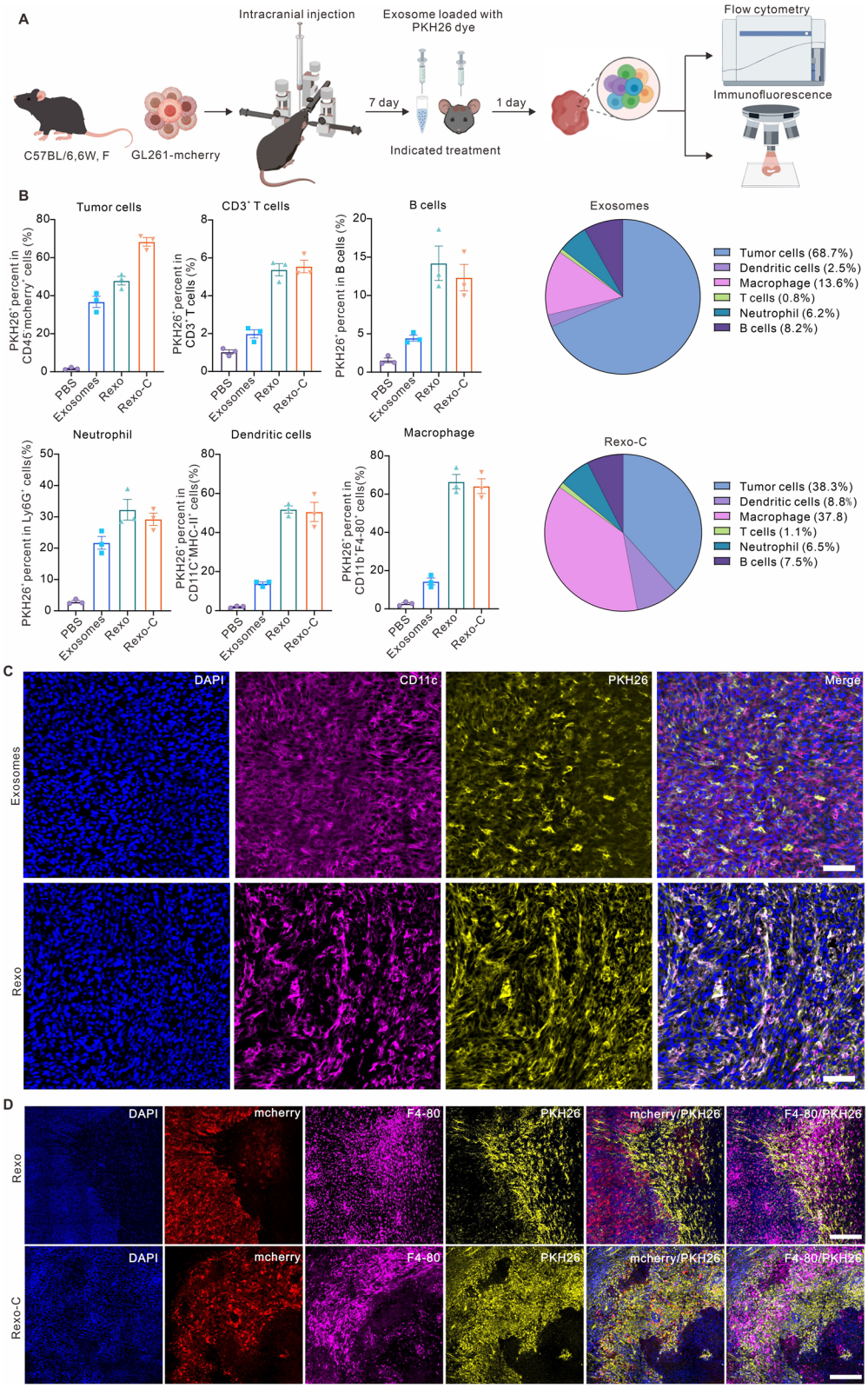

Fig. 6 (See legend on previous page.)

pathway and NF-κB pathway in BafA1@Rexo-SC results in the generation of "Lto", the release of VEGFA for high endothelial microvessel formation, and the release of chemokines for T and B cell recruitment. This approach not only promotes macrophage phagocytosis of tumor cells by blocking CD47 but also enhances effector T cell function through the release of type I interferon.

The in vivo results are particularly promising, with BafA1@Rexo-SC significantly prolonging survival rates in orthotopic glioma model mice and inducing complete tumor remission in a subset of animals. The system's ability to reverse the immunosuppressive GME, as evidenced by the reduction of M2-type macrophages/microglia and the increased infiltration of effector T cells, positions BafA1@Rexo-SC as a potent candidate for clinical translation in GBM treatment. To address potential safety concerns regarding immune overactivation in the central nervous system, future clinical translation will incorporate stringent safety assessments. These include dose-escalation studies in non-human primates to establish safe dosing thresholds, real-time monitoring of neuroinflammatory biomarkers in cerebrospinal fluid, and advanced imaging techniques to detect early signs of neurotoxicity. Furthermore, localized delivery via convection-enhanced delivery systems will minimize systemic exposure while maximizing tumor-targeted effects.

In summary, BafA1@Rexo-SC represents a novel therapeutic modality that harnesses the power of engineered exosomes to activate intrinsic immune pathways, reverse immunosuppression, and induce TLS formation within the GME. This study provides a foundation for further investigation into the clinical potential of BafA1@Rexo-SC in enhancing immunotherapy for glioma patients, offering a promising avenue for improving treatment outcomes in this aggressive form of cancer.

Experiment and method

materials

The medium of cell culture was purchased from Gibco Life Technologies, Inc. (Grand Island, NY, USA), including Modifed Eagle's Medium (DMEM), Roswell Park Memorial Institute (RPMI)-1640 medium. Fetal Bovine Serum (FBS) was obtained from Zhejiang Tianhang Biotechnology Co., Ltd. (Huzhou, China). Plasmocin was bought from InvivoGene (Toulouse, France) and penicillin/streptomycin was obtained from Biosharp (Hefei, China). Sterile 1 × phosphate bufered saline was purchased from Gibco Life Technologies, Inc. (Grand Island, NY, USA). All the cytokines were purchased from Biolegend (San Diego, CA, USA), containing granulocytemacrophage colony-stimulating factor macrophage colony-stimulating factor, interleukin-4, interleukin-13, and interferon-γ. BafA1 was bought from MCE (cat number: HY-100558). Acetonitrile, methanol and chloroform for High Performance Liquid Chromatography (HPLC) were all purchased from Termo Fisher Scientifc (Waltham, MA, USA) and their purity was more than 99%. The fuorescence dye PKH26 and PKH67 were obtained from MedChemExpress (NJ, USA). Radioimmunoprecipitation assay buffer and the inhibitors of protease and phosphatase were obtained from Beyotime (Shanghai, China). For western blot, primary antibodies STING, p-STING, NFκB and p-NFκB were purchased from ABclonal (Boston, MA, USA) and GAPDH, CD63, CD81 and Alix were obtained from Proteintech Group, Inc. (Chicago, IL, USA). Secondary antibodies goat anti-mouse IgG H&L-HRP conjugated and goat anti-rabbit IgG H&L-HRP conjugated were bought from Abcam (Cambridge, UK). Collagenase IV, neutral proteases and papain were purchased from Biosharp (Hefei, China). All the antibodies for fow cytometry and immunofluorescence were bought from Biolegend (San Diego, CA, USA).

Bioinformatics analysis

The bulk RNA-seq profiles of GBM data and match normal human tissue data were obtained from CGGA database. The expression profiles were transferred to transcripts per kilobase million (TPM) format, and the $\log_2(\mathrm{TPM}+0.001)$ format data were used for subsequent analysis. The Seurat package RunUMAP function was used to downscale the data through the UMAP (Uniform Manifold Approximation and Projection) algorithm to distinguish between different cell clusters. DimPlot function was used to visualize the distribution of immune cell types in tumor tissues in the STING high

(See figure on next page.)

Fig. 7 In vivo validation of the therapeutic potential and TLS formation ability of BafA1@Rexo-SC against glioma. **A** Diagram illustrating the treatment process, imaging process and experiment process for the established intracranial GBM model (GL261-luciferase) by intracranial injection of different engineered exosomes of varying equal mass. **B** Live imaging of small animals to track glioma progression in different treatment groups over time. **C** Analysis of the survival rates in the GL261 in situ mouse model (n = 8 for each group). **D** Statistics graph of body weight changes with intracranial injection of GL261 tumor cell after indicated treatment (n = 8). **E** Immunofluorescence to demonstrate the HEV formation in the indicated treatment groups. Scale bar: 100 μm. **F** Immunofluorescence to assess the TLS formation in the indicated treatment groups. Scale bar: 200 μm. Statistical analysis was performed using log-rank Mantel-Cox test for **C**. Data are presented as the mean ± SD. $^{*}P < 0.05$,$^{**}P < 0.01$, $^{***}P < 0.001$, and *NS* not significant

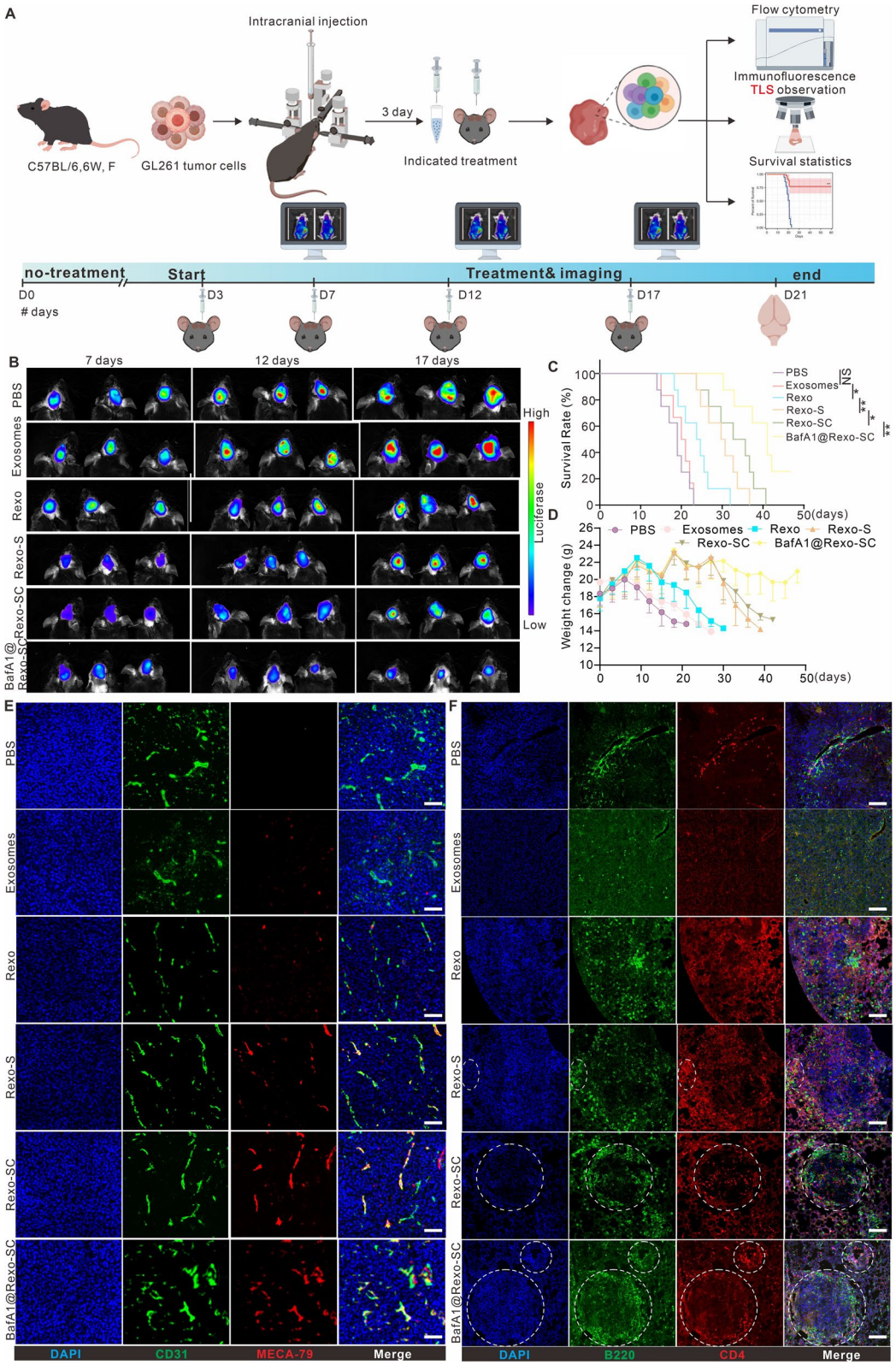

Fig. 7 (See legend on previous page.)

expression group and low expression group. The ggplot function of the ggplot2 package was used to demonstrate the difference in the number of immune cells in tumor tissues between the STING high expression group and the low expression group. The Seurat package FeaturePlot function were used to demonstration of chemokine expression in different cell populations after UMAP downscaling. Seurat package DotPlot function was used to demonstration of chemokine expression in tumor tissues of STING high and low expression groups in different cell types. All these analyses were performed in R (4.2.2).

Cell lines

Mouse BV2 cells, Raw264.7 cells and glioma cell line GL261 were obtained from the China Center for Type Culture Collection (Wuhan, China). The GL261-luciferase and GL261-mcherry were established in the lab. All cell lines were treated with 25 μg mL^{-1} Plasmocin (InvivoGene, Toulouse, France) for at least two weeks and were mycoplasmanegative as determined by MycoProbe Mycoplasma Detection Kit (R&DSystems, Minneapolis, MN, USA). Cells were grown in DMEM containing 10% FBS and 1% penicillin/streptomycin solution. Murine MSCs were purchased from Pro-cell (Cat number # CP-M131) and cultured in Complete medium (specifically designed for mouse MSCs, purchased from Procell) containing 10% (v/v) FBS and 1% (v/v) penicillin/streptomycin. Selection of murine MSC-nCD47, MSC-STING or MSC-STING/nCD47 were maintained with 100 pg/ml G418 (Sigma-Aldrich). Bone marrow-derived dendritic cells and macrophage (BMDC & BMDM) from C57BL/6 J mice were generated as previous descriptions in RPMI 1640 medium [39]. All the mediums were added with 10% (v/v) FBS and 100 μg mL^{-1} penicillin/streptomycin.

Lentivirus Construction and MSCs Transfection

The DNA sequences for nCD47-GFP-GPI expression are listed in the supporting information, mainly comprising the sequences for the signal peptide (MASPLTRFLSLNLLLLGESIILGSGEA), anti-CD47 nanobody, EGFP, and a GPI anchor. Lentivirus containing a purinomycin resistance gene was constructed by Shanghai Jikai Biotechnology Co., LTD. The virus titer used to transfect MSCs was 1×10^7.

Identify The Location Of nCD47 and STING protein

MSCs were seeded in a glass-bottom cell culture dish (NEST, catalog no. 801001; 1×10^5 per well) and were washed with PBS and fixed in 4% paraformaldehyde for 30 min and then washed in PBS again. Cells were incubated with DAPI and primary anti-STING antibody with following incubated with Cy5 labeled goat anti-rabbit IgG.

before imaged by confocal laser scanning microscopy (LSM 710). The images were processed by image J.

Preparation of Exosomes and Other Engineered Rexo

In 10 cm cell culture dishes, 6×10^6 MSCs were planted and irradiated with a single dose of 20 Gy using X-rays (ChiRad160, Dandong Aolong Radiative Instrument Group Co., Ltd, dose rate 2 Gy/min, field size covering the entire culture dish)(Irradiation can be avoided when purifying exosomes). Next, the medium of irradiated cells was renewed by 20 mL completed medium which its exosomes had been removed via centrifugation. 72 h later, the medium was collected, and cell debris were removed by 2000 g for 20 min and 10,000 g for

(See figure on next page.)

Fig. 8 Validation of the ability of BafA1@Rexo-SC to reverse the GME. **A** Identification of the proportion of B cell in different given treatment groups (n = 6 for each group). **B** Identification of the proportion of M2 macrophage in different given treatment groups (n = 6 for each group). **C** Identification of the proportion of activated DC cells in different given treatment groups (n = 6 for each group). **D** Identification of the proportion of IFN-γ-positive CD8 T cells in different given treatment groups (n = 6 for each group). **E** Identification of the proportion of central memory $CD8^+$ T cells in different given treatment groups (n = 6 for each group). **F** Identification of the proportion of exhausting precursor $CD8^+$ T cells in different given treatment groups (n = 6 for each group).(G) Identification of the proportion of $CD8^+$ T cells in different given treatment groups (n = 6 for each group). **H** Identification of the proportion of $CD4^+$ T cells in different given treatment groups (n = 6 for each group). **I** Identification of interferon type I and type II content in the lysed supernatant of the mouse brain in different given treatment groups (n = 6 for each group). **J** Identification of TNF-α content in the lysed supernatant of the mouse brain in different given treatment groups (n = 6 for each group). **K** Determination of VEGFA in mouse brain lysate supernatant in different given treatment groups (n = 6 for each group). **L** Determination of CXCL9 in mouse brain lysate supernatant in different given treatment groups (n = 6 for each group). **M** Determination of CXCL10 in mouse brain lysate supernatant in different given treatment groups (n = 6 for each group). **N** Determination of CXCL12 in mouse brain lysate supernatant in different given treatment groups (n = 6 for each group). **O** Determination of CXCL13 in mouse brain lysate supernatant in different given treatment groups (n = 6 for each group). **P** Immunofluorescence to identify that intracranial injection of BafA1@Rexo-SC promotes the uptake of tumor cells by macrophages, with a scale bar of 100 μm. **Q** Immunofluorescence to identify that intracranial injection of BafA1@Rexo-SC promotes the uptake of tumor cells by DCs and the interaction between DCs and $CD8^+$T cells, with a scale bar of 100 μm. Statistical analysis was performed using one-way ANOVA with Tukey's multiple comparison test. Data are presented as the mean ± SD. *$P < 0.05$,**$P < 0.01$, ***$P < 0.001$, and *NS* not significant

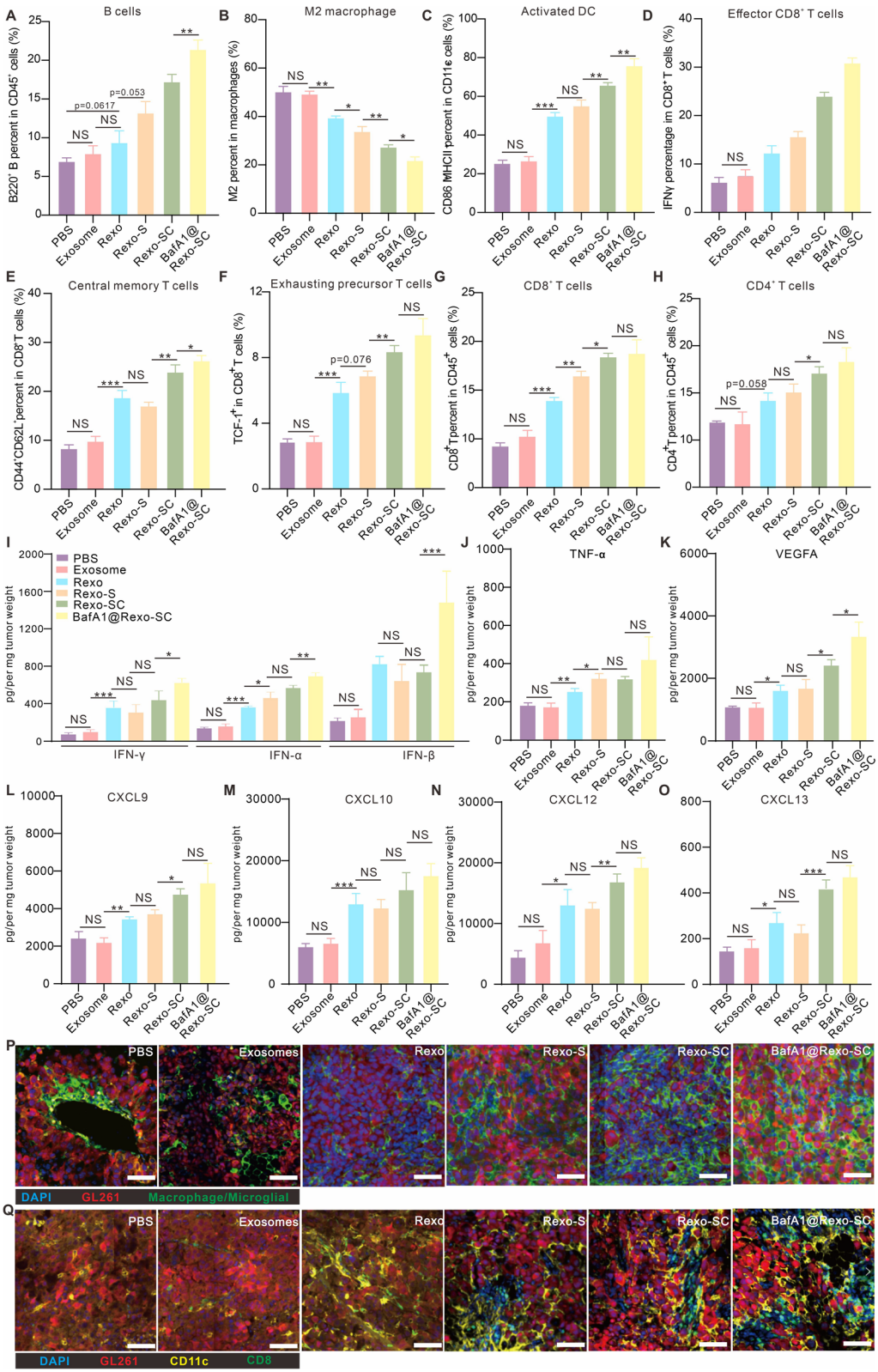

Fig. 8 (See legend on previous page.)

30 min followed filtration using a 0.22 μm membrane. Exosomes and other engineered Rexo were gained from the supernatant via 11,0000 g for further 70 min at 4 °C and washed with sterile 1 × PBS for 2 times. At last, the exosomes and other engineered Rexo were resuspended with 1 × PBS for subsequent experiments. To obtain BafA1@Rexo-SC, a 5 μM concentration of BafA1 needs to be added to the culture medium after radiotherapy and co-incubated with MSCs for 72 h.

Quantification of exosomes and other engineered rexo

The protein concentrations of exosomes and other engineered Rexo were measured. After washing, exosomes and other engineered Rexo were lysed with radioimmunoprecipitation assay (RIPA) buffer at 4 °C for 30 min and then centrifuged for 30 min at 12, 000 g at 4 °C. The supernatant containing the total protein was transferred to a new centrifuge tube. Protein was quantified using the BCA Protein Assay Kit (Thermo Fisher Scientific) in accordance with the manufacturer's protocol.

Characterization of exosomes size, zeta potential and transmission electron microscopy (TEM) determination

One milliliter of 30 ng mL^{-1} exosomes or other engineered Rexo were taken for the measurement of the particle size, polydispersity index and zeta potential by Malvern laser particle size analyzer (Zetasizer Nano ZSP). For further identifcation of the sizes and morphology of exosomes or other engineered Rexo were washed by ddH_2O, deposited on copper mesh and then observed by TEM (HT7700-SS/FEI Tecnai G20 TWIN).

Western blotting

All the exosomes and cells were lysed by RIPA bufer with the inhibitors of protease and phosphatase at 4 °C for 30 min, and then centrifuged at 12,000*g* for 30 min at 4 °C. Te mass of the sample loading was adjusted to the same according to their protein concentrations that were detected by BCA Protein Assay Kit. The samples were separated by SDS-PAGE and transferred to polyvinylidene difuoride membrane after boiled for 5 min. The membranes block by 5% not-fat milk at room temperature for 1 h and incubated with related primary antibodies at 4 °C overnight. With several wash by Tris-bufered saline with 0.05% Tween-20, secondary antibodies incubated with the membranes at room temperature for 1 h. NcmECL Ultra (P10100, NCM Biotech) was applied for chemiluminescent exposure of the blot.

Analysis of BafA1 loaded in BafA1@Rexo-SC in vitro by HPLC

Ultrasound of BafA1@Rexo-SC was performed in methanol solution following centrifugation (11,0000*g*, 30 min). Then, the supernatants were filtered (0.2 μm filters) for HPLC (LC-2030C Plus, designed by Shimadzu Corporation in Japan). A C18 (250 × 4.6 mm, 5 μm particle size) HPLC packed column was used as the chromatographic column. The mobile phase was CH3OH 0.5%TFA/H_2O 0.5% TFA (1:1, *V/V*), the flow rate was 1.0 mL min^{-1}, and the detection wavelength was 254 nm.

In Vitro cellular uptake assay

To determine the cellular co-localization of exosomes or engineered exosomes, M2 type BMDM, BMDC and GL261cells were seeded in a glass-bottom cell culture dish (NEST, catalog no. 801001; 1×10^5 per well) and incubated with PKH26-labeled exosomes or engineered exosomes for 24 h. In addition, to show the location of the cell membrane, BMDM and BMDC labeled the cell membrane using PKH26 dye, and also used Alexa Fluor®647 anti-mouse CD47 antibody (purchased from biolegend, cat# 127509) to label the CD47 marker expressed in GL261. Subsequently, these cells were washed three times in PBS and fixed in 4% paraformaldehyde for 30 min, and then stained with DAPI for 10 min. After that, cells were washed with PBS again. Cells were imaged by confocal laser scanning microscopy (LSM 710). For quantitative assessment of cellular uptake, cells were seeded in six-well cell culture dishes and treated as above, then washed in PBS three times, collected, fixed, and resuspended in PBS (150 μL) for flow cytometry detection.

Cytokines detection

GL261 tumors from mice were grinded into homogenate. The supernatant was collected by 6000 g centrifugation for 20 min at 4 °C. Te LEGENDplex Mouse Cytokine Release Syndrome Panel (13-plex) with VBottom Plate (purchased from Biolegend) or Elisa kit for Chemokines and growth factors was used for cytokine detection.

RNA sequencing (RNA-seq)

Total RNA was isolated from the BMDM treated with exosomes or other engineered Rexo using Trizol reagent following the manufacturer's specified instructions. RNA-seq sequencing services were executed proficiently by BGI Genomics Co., Ltd (Wuhan, China).

Mice

C57BL/6 J female mice were obtained from Hunan Slyke Jingda Laboratory Animal Co. Ltd. in Hunan, China. These mice were bred and maintained in a specific pathogen-free (SPF) barrier facility.

In vivo cellular internalization assay

To identify exosomes or other engineered Rexo uptake by cells in tumor *in vivo*, we intracranial injected 5 μL PKH26 marked exosomes or other engineered Rexo to mice with GL261 tumor burden. 24 h later, the mice were sacrifced and the tumors were digested into single cell for fow cytometry analysis before they were incubated with antibodies of CD45 (clone S18009F), CD3 (clone 17A2), B220 (clone RA3-6B2), CD11b (clone M1/70), Ly6G (clone S19018G), F4/80 (clone BM8), CD206 (clone C068C2), CD11c (clone N418), MHCII (clone M5/114.15.2) and NK1.1 (clone PK136). Besides, some tumor tissues were fxed, dehydrated and sectioned into frozen sections which were going to stain by related antibodies and observed via confocal laser scanning microscopy.

Tissue immunofluorescent staining

Tumor tissues were fixed, embedded in paraffin, and sectioned with a microtome. The sections were then dewaxed and hydrated routinely. Antigen retrieval was achieved by applying a Tris–EDTA Buffer solution, and endogenous peroxidases were quenched using 3% H_2O_2. Samples were subsequently blocked with normal goat serum. The slides were incubated overnight with the following antibodies: Alexa Fluor® 647 anti-mouse CD11c Antibody (Biolegend, cat# 117312), Alexa Fluor® 594 anti-mouse F4/80 Antibody (Biolegend, cat# 123140), Alexa Fluor® 488 anti-mouse CD8a Antibody (Biolegend, cat# 100723). Subsequently, DAPI was applied for 20 min at room temperature. Finally, tissue immunofluorescence was analyzed using the confocal laser scanning microscopy.

Animal model experiments and evaluation of therapeutic effects

To establish the GBM model in brain, C57BL/6 J female mice (6–8 weeks old) were anesthetized with a 1% pentobarbital sodium solution before all surgical procedures. GL261-luciferase (LUC) cells (1×10^6 cells suspended in 10 μL of PBS) were stereotactically injected into the right ventricle's striatum. The rate of transfection for GL261 was 1 μL/min, and the total volume was 10 μL. Seven days, twelve days and seventeen days after the inoculation with GL261-luciferase cells, each mouse underwent bioluminescence imaging to ensure the successful and uniform establishment of the GBM model. Subsequently, the mice were randomly divided into six groups: PBS, Exosomes, Rexo, Rexo-S, Rexo-SC and BafA1@Rexo-SC, and were given their respective treatments. The rate of transfection for different MSCs was 1 μL/min, and the total volume was 10 μL.To assess the development of the GBM model, eight mice in each group were imaged on the day when all treatments were completed under 1% pentobarbital sodium anesthesia using the Bruker In Vivo MS FX PRO Imager.

Bioluminescence imaging

After anesthetizing C57BL/6 J female mice (6–8 weeks old) with 1% pentobarbital sodium, they were intraperitoneally injected with firefly luciferin (150 mg $kg-1$; Sigma-Aldrich; CAS: 103404–75-7). After 15 min, mice were imaged using the Bruker In Vivo MS FX PRO Imager with 3 min exposure times for acquiring luminescent images.

Collection of tumor-infiltrating immunocytes

Tumor-infiltrating immune cells were obtained from the GBM model as previously described [40].

Flow cytometry

For cell-surface analysis, cells were stained with the anti-mouse Zombie NIR Fixable Viability Kit (423,106) and incubated with antibodies against CD45 (103114), B220 (103225), CD11b (101205), CD86 (105018), MHC-II (116418), CD44 (103044), CD62L (161213), PD-1 (109112), F4/80 (123121), CD3 (100212), CD4 (100408), and CD8a (100752) at the recommended concentrations. Incubation was carried out at 4 °C for 30 min. For T-cell intracellular IFN-γ (505808) cytokine staining, cells were fixed and permeabilized after stimulation with Phorbol 12-myristate 13-acetate (PMA) (ab120297, Abcam, 100 ng $mL-1$), Monensin sodium salt (ab120499, Abcam, 1 ug $mL-1$), and Ionomycin calcium salt (5608212, PeproTech, 100 ng $mL-1$) for 3 h. For CD206 (141706) and TCF-1 (655203) staining, cells were also fixed and permeabilized. All flow cytometry antibodies were purchased from Biolegend (San Diego, CA, USA).

Statistical analysis

The unpaired two-tailed Student's *t* test to compare the differences between the two groups was used, while survival rates were evaluated with the log-rank Mantel-Cox test using GraphPad Prism 7 software. Repeated measurements of tumor volume growth were compared using a One-way analysis of variance (ANOVA). Flow cytometry data were analyzed using FlowJo.10. Significant differences between the groups are indicated by $^*p < 0.05$, $^{**}p < 0.01$, and $^{***}p < 0.001$, and NS, not significant.

Supplementary Information

The online version contains supplementary material available at https://doi.org/10.1186/s12951-025-03301-5.

Additional file1 (DOCX 932 KB)

Acknowledgements
We thank the Optical Bioimaging Core Facility of WNLO-HUST for the support in data acquisition.

Author contributions
Man.Li. and Lisen.Lu. designed the research. Qiuhong.Bao., Minghui. Zhou., Bin.Nie., Yanchao.Liu., Kai. Shu. and Ting. Lei. performed experiments and analyzed data. Lisen.Lu., Qiuhong.Bao. and Minghui. Zhou. provided resources or conducted experiments. Man.Li., Lisen.Lu. and Mingxin.Zhu. wrote the manuscript and prepared all fgures. All authors reviewed the manuscript.

Funding
This research was supported by the National Natural Science Foundation of China (No. 82001193, No. 82102900) and the China postdoctoral Science Foundation (2023M731223, 2023T160253).

Data availability
No datasets were generated or analysed during the current study.

Declarations

Conflict of interest
The authors declare no competing interests.

Ethical approval and consent to participate
All animal studies were conducted under the approval of the Hubei Provincial Animal Care and Use Committee and followed the experimental guidelines established by the Animal Experimentation Ethics Committee of Huazhong University of Science and Technology. This study was approved by the Ethics Committee of Huazhong University of Science & Technology (IRB ID: TJ20170201).

Author details
[1]Department of Neurosurgery, Tongji Hospital, Tongji Medical College, Huazhong University of Science and Technology, Wuhan, People's Republic of China. [2]Department of Anesthesiology and Pain Medicine, Hubei Key Laboratory of Geriatric Anesthesia and Perioperative Brain Health, and Wuhan Clinical Research Center for Geriatric Anesthesia, Tongji Hospital, Tongji Medical College, Huazhong University of Science and Technology, Wuhan, People's Republic of China. [3]College of Biomedicine and Health and College of Life Science and Technology, Huazhong Agricultural University, Wuhan 430070, People's Republic of China. [4]Department of Oncology Medicine, Tiantai People's Hospital of Zhejiang Province, Tiantai 317200, Zhejiang Province, China.

Received: 11 January 2025 Accepted: 6 March 2025
Published online: 22 March 2025

References

1. Liu J, Peng J, Jiang J, Liu Y. Clinical immunotherapy in glioma: current concepts, challenges, and future perspectives. Front Immunol. 2024;1(15):1476436.
2. Rong L, Li N, Zhang Z. Emerging therapies for glioblastoma: current state and future directions. J Exp Clin Cancer Res. 2022;41(1):142.
3. van den Bent MJ, Geurts M, French PJ, Smits M, Capper D, Bromberg JEC, Chang SM. Primary brain tumours in adults. Lancet. 2023;402(10412):1564–79.
4. Klemm F, Maas RR, Bowman RL, Kornete M, Soukup K, Nassiri S, Brouland JP, Iacobuzio-Donahue CA, Brennan C, Tabar V, Gutin PH, Daniel RT, Hegi ME, Joyce JA. Interrogation of the microenvironmental landscape in brain tumors reveals disease-specific alterations of immune cells. Cell. 2020;181(7):1643-1660.e17.
5. Mellman I, Chen DS, Powles T, Turley SJ. The cancer-immunity cycle: indication, genotype, and immunotype. Immunity. 2023;56(10):2188–205.
6. Schumacher TN, Thommen DS. Tertiary lymphoid structures in cancer. Science. 2022;375(6576):eabf9419.
7. Teillaud JL, Houel A, Panouillot M, Riffard C, Dieu-Nosjean MC. Tertiary lymphoid structures in anticancer immunity. Nat Rev Cancer. 2024;24(9):629–46.
8. Cabrita R, Lauss M, Sanna A, Donia M, Skaarup Larsen M, Mitra S, Johansson I, Phung B, Harbst K, Vallon-Christersson J, van Schoiack A, Lövgren K, Warren S, Jirström K, Olsson H, Pietras K, Ingvar C, Isaksson K, Schadendorf D, Schmidt H, Bastholt L, Carneiro A, Wargo JA, Svane IM, Jönsson G. Tertiary lymphoid structures improve immunotherapy and survival in melanoma. Nature. 2020;577(7791):561–5.
9. Shen S, Cui Y, Li M, Yu K, Zhu Q, Zhang X, Shen W, Li H, Jiang H, Li M, Wang X, Zhao X, Ren X, Lin S. TLR agonists promote formation of tertiary lymphoid structure and improve anti-glioma immunity. Neuro Oncol. 2024;27:noae167.
10. Ramachandran M, Vaccaro A, van de Walle T, Georganaki M, Lugano R, Vemuri K, Kourougkiaouri D, Vazaios K, Hedlund M, Tsaridou G, Uhrbom L, Pietilä I, Martikainen M, van Hooren L, Olsson Bontell T, Jakola AS, Yu D, Westermark B, Essand M, Dimberg A. Tailoring vascular phenotype through AAV therapy promotes anti-tumor immunity in glioma. Cancer Cell. 2023;41(6):1134-1151.e10.
11. Jiang N, Xie B, Xiao W, Fan M, Xu S, Duan Y, Hamsafar Y, Evans AC, Huang J, Zhou W, Lin X, Ye N, Wanggou S, Chen W, Jing D, Fragoso RC, Dugger BN, Wilson PF, Coleman MA, Xia S, Li X, Sun LQ, Monjazeb AM, Wang A, Murphy WJ, Kung HJ, Lam KS, Chen HW, Li JJ. Fatty acid oxidation fuels glioblastoma radioresistance with CD47-mediated immune evasion. Nat Commun. 2022;13(1):1511.
12. Low JT, Chandramohan V, Bowie ML, Brown MC, Waitkus MS, Briley A, Stevenson K, Fuller R, Reitman ZJ, Muscat AM, Hariharan S, Hostettler J, Danehower S, Baker A, Khasraw M, Wong NC, Gregory S, Nair SK, Heimberger A, Gromeier M, Bigner DD, Ashley DM. Epigenetic STING silencing is developmentally conserved in gliomas and can be rescued by methyltransferase inhibition. Cancer Cell. 2022;40(5):439–40.
13. Wang Y, Luo J, Alu A, Han X, Wei Y, Wei X. cGAS-STING pathway in cancer biotherapy. Mol Cancer. 2020;19(1):136.
14. Reisländer T, Groelly FJ, Tarsounas M. DNA Damage and cancer immunotherapy: a STING in the tale. Mol Cell. 2020;80(1):21–8.
15. Concannon K, Morris BB, Gay CM, Byers LA. Combining targeted DNA repair inhibition and immune-oncology approaches for enhanced tumor control. Mol Cell. 2023;83(5):660–80.
16. Zhang L, Jiang C, Zhong Y, Sun K, Jing H, Song J, Xie J, Zhou Y, Tian M, Zhang C, Sun X, Wang S, Cheng X, Zhang Y, Wei W, Li X, Fu B, Feng P, Wu B, Shu HB, Zhang J. STING is a cell-intrinsic metabolic checkpoint restricting aerobic glycolysis by targeting HK2. Nat Cell Biol. 2023;25(8):1208–22.
17. Ding F, Liu J, Ai K, Xu C, Mao X, Liu Z, Xiao H. Simultaneous activation of pyroptosis and cGAS-STING pathway with epigenetic/photodynamic nanotheranostic for enhanced tumor photoimmunotherapy. Adv Mater. 2024;36(7): e2306419.
18. Huang Y, Shi Y, Wang Q, Qi T, Fu X, Gu Z, Zhang Y, Zhai G, Zhao X, Sun Q, Lin G. Enzyme responsiveness enhances the specificity and effectiveness of nanoparticles for the treatment of B16F10 melanoma. J Control Release. 2019;28(316):208–22.
19. Li M, Sun S, Dangelmajer S, Zhang Q, Wang J, Hu F, Dong F, Kahlert UD, Zhu M, Lei T. Exploiting tumor-intrinsic signals to induce mesenchymal stem cell-mediated suicide gene therapy to fight malignant glioma. Stem Cell Res Ther. 2019;10(1):88.
20. Li M, Zeng L, Liu S, Dangelmajer S, Kahlert UD, Huang H, Han Y, Chi X, Zhu M, Lei T. Transforming growth factor-β promotes homing and therapeutic efficacy of human mesenchymal stem cells to glioblastoma. J Neuropathol Exp Neurol. 2019;78(4):315–25.
21. Li M, Lu L, Xiao Q, Maalim AA, Nie B, Liu Y, Kahlert UD, Shu K, Lei T, Zhu M. Bioengineer mesenchymal stem cell for treatment of glioma by IL-12 mediated microenvironment reprogramming and nCD47-SLAMF7 mediated phagocytosis regulation of macrophages. Exploration. 2024;4:20240027.
22. Jiang W, Xu J. Immune modulation by mesenchymal stem cells. Cell Prolif. 2020;53(1): e12712.

23. Lin Z, Wu Y, Xu Y, Li G, Li Z, Liu T. Mesenchymal stem cell-derived exosomes in cancer therapy resistance: recent advances and therapeutic potential. Mol Cancer. 2022;21(1):179.
24. Zhang F, Guo J, Zhang Z, Qian Y, Wang G, Duan M, Zhao H, Yang Z, Jiang X. Mesenchymal stem cell-derived exosome: a tumor regulator and carrier for targeted tumor therapy. Cancer Lett. 2022;1(526):29–40.
25. Gao Y, Zheng X, Chang B, Lin Y, Huang X, Wang W, Ding S, Zhan W, Wang S, Xiao B, Huo L, Yu Y, Chen Y, Gong R, Wu Y, Zhang R, Zhong L, Wang X, Chen Q, Gao S, Jiang Z, Wei D, Kang T. Intercellular transfer of activated STING triggered by RAB22A-mediated non-canonical autophagy promotes antitumor immunity. Cell Res. 2022;32(12):1086–104.
26. Kuchitsu Y, Mukai K, Uematsu R, Takaada Y, Shinojima A, Shindo R, Shoji T, Hamano S, Ogawa E, Sato R, Miyake K, Kato A, Kawaguchi Y, Nishitani-Isa M, Izawa K, Nishikomori R, Yasumi T, Suzuki T, Dohmae N, Uemura T, Barber GN, Arai H, Waguri S, Taguchi T. STING signalling is terminated through ESCRT-dependent microautophagy of vesicles originating from recycling endosomes. Nat Cell Biol. 2023;25(3):453–66.
27. Wan C, Sun Y, Tian Y, Lu L, Dai X, Meng J, Huang J, He Q, Wu B, Zhang Z, Jiang K, Hu D, Wu G, Lovell JF, Jin H, Yang K. Irradiated tumor cell-derived microparticles mediate tumor eradication via cell killing and immune reprogramming. Sci Adv. 2020;6(13):eaay9789.
28. Hu Y, Sun Y, Liao Z, An D, Liu X, Yang X, Tian Y, Deng S, Meng J, Wang Y, Li J, Deng Y, Zhou Z, Chen Q, Ye Y, Wei W, Wu B, Lovell JF, Jin H, Huang F, Wan C, Yang K. Irradiated engineered tumor cell-derived microparticles remodel the tumor immune microenvironment and enhance antitumor immunity. Mol Ther. 2024;32(2):411–25.
29. Huang Y, Gu Z, Fan Y, Zhai G, Zhao X, Sun Q, Shi Y, Lin G. Inhibition of the adenosinergic pathway: the indispensable part of oncological therapy in the future. Purinergic Signal. 2019;15(1):53–67.
30. Feng Q, Ma X, Cheng K, Liu G, Li Y, Yue Y, Liang J, Zhang L, Zhang T, Wang X, Gao X, Nie G, Zhao X. Engineered Bacterial outer membrane vesicles as controllable two-way adaptors to activate macrophage phagocytosis for improved tumor immunotherapy. Adv Mater. 2022;34(40): e2206200.
31. Zhang P, Rashidi A, Zhao J, Silvers C, Wang H, Castro B, Ellingwood A, Han Y, Lopez-Rosas A, Zannikou M, Dmello C, Levine R, Xiao T, Cordero A, Sonabend AM, Balyasnikova IV, Lee-Chang C, Miska J, Lesniak MS. STING agonist-loaded, CD47/PD-L1-targeting nanoparticles potentiate antitumor immunity and radiotherapy for glioblastoma. Nat Commun. 2023;14(1):1610.
32. Zhao R, Zhang J, Ma J, Qu Y, Yang Z, Yin Z, Li F, Dong Z, Sun Q, Zhu S, Chen ZJ, Gao D. cGAS-activated endothelial cell-T cell cross-talk initiates tertiary lymphoid structure formation. Sci Immunol. 2024;9(98):eadk2612.
33. Sun Y, Hu H, Liu Z, Xu J, Gao Y, Zhan X, Zhou S, Zhong W, Wu D, Wang P, Rao Z, Kong L, Zhou H. Macrophage STING signaling promotes NK cell to suppress colorectal cancer liver metastasis via 4–1BBL/4-1BB co-stimulation. J Immunother Cancer. 2023;11(3): e006481.
34. Zhao Z, Zhang KN, Wang Q, Li G, Zeng F, Zhang Y, Wu F, Chai R, Wang Z, Zhang C, Zhang W, Bao Z, Jiang T. Chinese glioma genome atlas (CGGA): a comprehensive resource with functional genomic data from Chinese Glioma patients. Genom Proteom Bioinform. 2021;19(1):1–12.
35. van Duijn A, Van der Burg SH, Scheeren FA. CD47/SIRPα axis: bridging innate and adaptive immunity. J Immunother Cancer. 2022;10(7): e004589.
36. Lin H, Liu C, Hu A, Zhang D, Yang H, Mao Y. Understanding the immunosuppressive microenvironment of glioma: mechanistic insights and clinical perspectives. J Hematol Oncol. 2024;17(1):31.
37. Vella G, Hua Y, Bergers G. High endothelial venules in cancer: regulation, function, and therapeutic implication. Cancer Cell. 2023;41(3):527–45.
38. Johansson-Percival A, He B, Li ZJ, Kjellén A, Russell K, Li J, Larma I, Ganss R. De novo induction of intratumoral lymphoid structures and vessel normalization enhances immunotherapy in resistant tumors. Nat Immunol. 2017;18(11):1207–17.
39. Qi S, Lu L, Zhou F, Chen Y, Xu M, Chen L, Yu X, Chen WR, Zhang Z. Neutrophil infiltration and whole-cell vaccine elicited by *N*-dihydrogalactochitosan combined with NIR phototherapy to enhance antitumor immune response and T cell immune memory. Theranostics. 2020;10(4):1814–32.
40. Lu L, Zi H, Zhou J, Huang J, Deng Z, Tang Z, Li L, Shi X, Lo PC, Lovell JF, Deng D, Wan C, Jin H. Engineered microparticles for treatment of murine brain metastasis by reprograming tumor microenvironment and inhibiting MAPK pathway. Adv Sci (Weinh). 2023;10(8): e2206212.

Publisher's Note